



HAL
open science

Increased Mg release rates and related Mg isotopic signatures during bacteria-phlogopite interactions

Clarisse Balland-Bolou-Bi, Emile Bolou-Bi, Nathalie Vigier, Christian Mustin,
Anne Poszwa

► To cite this version:

Clarisse Balland-Bolou-Bi, Emile Bolou-Bi, Nathalie Vigier, Christian Mustin, Anne Poszwa. Increased Mg release rates and related Mg isotopic signatures during bacteria-phlogopite interactions. *Chemical Geology*, 2019, 506, pp.17-28. 10.1016/j.chemgeo.2018.12.020 . hal-01968263

HAL Id: hal-01968263

<https://hal.science/hal-01968263>

Submitted on 19 Oct 2021

HAL is a multi-disciplinary open access archive for the deposit and dissemination of scientific research documents, whether they are published or not. The documents may come from teaching and research institutions in France or abroad, or from public or private research centers.

L'archive ouverte pluridisciplinaire **HAL**, est destinée au dépôt et à la diffusion de documents scientifiques de niveau recherche, publiés ou non, émanant des établissements d'enseignement et de recherche français ou étrangers, des laboratoires publics ou privés.



Distributed under a Creative Commons Attribution - NonCommercial 4.0 International License

30 the initial phlogopite, while its binding to organics is expected to be related to its preferential
31 enrichment in heavy isotopes. Despite its small range of variations, the $\delta^{26}\text{Mg}$ values of
32 solutions vary inversely with pH, thus suggesting that secondary phases preferentially
33 enriched in ^{26}Mg at the highest pH values may play a key role.

34

35 *Keywords: Phlogopite, Bacteria, Organic acids, Magnesium stable isotopes*

36 1. INTRODUCTION

37 Silicate minerals, which are a major component of the continental crust, represent the main
38 reservoir of magnesium and calcium on the Earth's surface. The reaction of atmospheric CO₂
39 with silicate minerals releases divalent cations (Mg²⁺ and Ca²⁺) into rivers, which will
40 ultimately form carbonates in the ocean. This process results in the net removal of CO₂ from
41 the atmosphere (Berner, 1992). Thus, at the global scale, silicate mineral weathering is linked
42 to the carbon cycle, and it therefore influences climate change on geological timescales. On
43 shorter timescales, the silicate-weathering rate can vary significantly, which may potentially
44 affect the carbon cycle (Bastian et al., 2017). At the soil scale, mineral weathering plays a key
45 role in soil genesis and vegetation growth by releasing elements and nutrients from minerals.
46 Silicate mineral weathering results from the combination of several steps, including physical
47 disintegration and chemical dissolution. Both processes are more or less linked to biological
48 processes induced by bacteria, which are rarely considered in geochemical or isotopic studies.
49 Many studies that have been carried out under experimental conditions have demonstrated
50 that bacteria can amplify silicate-weathering reactions (Barker and Banfield, 1998; Hutchens
51 et al., 2003; Leyval et al., 1990; Robert and Berthelin, 1986; Welch and Ullman, 1999). Some
52 bacteria from diverse genera are characterized by their ability to solubilize minerals, as
53 reported in the review of Uroz et al., 2009. However, previous studies have not indicated
54 whether silicate dissolution represents an indirect consequence of microbial metabolism (i.e.,
55 the release of protons, metabolites or specific ligands), or if it depends on a specific strategy
56 (e.g., if dissolution serves some physiological function) that gives a competitive ecological
57 advantage to colonizing bacteria (Bennett et al., 2001). Few studies have focused on the
58 quantitative and qualitative impact of microbial diversity on silicate weathering in soils
59 (Bennett et al., 2001, 1996; Rogers and Bennett, 2004). Most experimental studies have
60 concluded that mineral chemistry strongly influences the colonization patterns of mineral and

61 rocks by bacteria, as well as their metabolic activities. These experimental investigations have
62 mainly been based on (1) analyses of cations released in solution by minerals and rocks, (2)
63 analyses of the structural and chemical modification of minerals observed using microscopy
64 or X-ray diffraction and (3) the bacterial colonization patterns of minerals. In these studies,
65 the direct effects of bacteria can hardly be distinguished from the indirect effects of the
66 metabolites produced by these bacteria.

67 Recently, the stable isotopic compositions of metals have been used as an innovative
68 tool to trace biogeochemical processes, including bacteria-mineral interactions, silicate
69 mineral weathering, and the sources and transportation of cations in rivers. For example, some
70 studies have shown that bacteria-mineral interaction processes can induce the fractionation of
71 the stable isotopes of transition metals (e.g., Zn, Fe, Cu) (Anbar, 2004; Beard, 1999; Beard et
72 al., 2003; Brantley et al., 2004, 2001; Mathur et al., 2005). In particular, these shifts are
73 observed during the bacteria- and ligand-promoted dissolution of Fe-containing minerals (i.e.,
74 hornblende or goethite): the Fe released into the solution by these phases is enriched in light
75 isotopes, with greater fractionation observed in the presence of strong ligands (Brantley et al.,
76 2004, 2001; Wiederhold et al., 2006). Redox reactions may also induce some isotope
77 fractionation in these transition elements (Wiederhold et al., 2006).

78 In contrast to these cations, magnesium is an element that is much less sensitive to
79 physicochemical conditions because it has an invariable oxidation state (+II). On the other
80 hand, it has been demonstrated that magnesium is one of the most important cations for
81 bacterial growth (Pelmont, 1993) because magnesium is essential for the normal cell division
82 of bacteria, and it stimulates the growth of these organisms (Maloney and Valvano, 2006).
83 Thus, Mg is the most abundant divalent metal in bacteria cells, and it is required for many
84 structural and enzymatic functions. At least three families of proteins function as magnesium
85 transporters for many strains of bacteria. In recent years, it has been shown that a subset of

86 these transport proteins in bacteria are regulated by magnesium-responsive genetic control
87 elements (Maguire, 2006; Wakeman et al., 2014). Consequently, bacterial processes in soil
88 can be traced using variations and applications of Mg stable isotope ratios. Indeed, recent
89 environmental applications of stable magnesium isotopes have demonstrated that this tool
90 represents a good tracer of weathering and some biological processes. In nature, Mg isotopic
91 compositions ($\delta^{26}\text{Mg}$) vary from +1.8 ‰ (granite) to -6 ‰ (carbonate) (Brenot et al., 2008;
92 Galy et al., 2002; Huang et al., 2012; Li et al., 2010; Liu et al., 2011; Pogge von Strandmann
93 et al., 2008). This indicates that the processes controlling the release of Mg from the
94 continental crust to the formation of carbonate in the ocean are associated with Mg isotopic
95 fractionation. Several studies have investigated the role of silicate weathering in both natural
96 ecosystems (Bolou-Bi et al., 2012; Brenot et al., 2008; ~~Mavromatis et al., 2012~~; Tipper et al.,
97 2010, 2008, 2006) and using experimental leaching and clay synthesis analyses (Ryu et al.,
98 2016; Wimpenny et al., 2014). Ryu et al., 2016 highlighted the dichotomy between the field
99 studies and experimental investigations of low-temperature processes. The role of biological
100 reactions in natural systems may partly explain this gap. A few studies have focused on the
101 role of vegetation (Black et al., 2008; Bolou-Bi et al., 2016, 2012, 2010). These authors
102 observed significant Mg isotopic fractionation between plants and their nutrient sources, in
103 which the enrichment of heavy isotopes in plants is mainly controlled by biogeochemical
104 processes at the root level. These results were obtained under both experimental conditions
105 and in the field, but they did not estimate the potential roles of microorganisms. Indeed, a
106 recent study (Fahad et al., 2016) has highlighted that fungi are able to fractionate Mg isotopes.
107 In addition, it could help clarify the relationships between microorganisms and soil
108 development.

109 The aim of this study was to experimentally investigate the impact of bacterial activity
110 on Mg isotope signatures during the weathering of phlogopite minerals in a closed system and

111 under aerobic conditions. Two types of leaching experiments were performed: (1) “biotic”
112 experiments, which occurred in the presence of bacterial strains and Mg-free nutritive media,
113 and (2) “abiotic” experiments, which were performed using nitric or organic acids in sterile
114 mineral media. The two main strategies developed by bacteria were investigated, namely,
115 proton-promoted dissolution and ligand-promoted dissolution.

116

117 **2. MATERIALS AND METHODS**

118 Several phlogopite leaching experiments were performed using 4 different bacterial
119 strains (“biotic” experiments), which were previously isolated from plant rhizospheres and
120 acidic soils. To compare and distinguish the particular chemical processes linked to the
121 weathering ability of each isolated bacterial strain, leaching experiments without bacteria
122 were also performed using various acids:

123 - citric acid (10^{-3} M, pH adjusted at 3.5 to 6)

124 - gluconic acid (10^{-3} M, pH adjusted at 3.5 and 5)

125 - nitric acid (concentration adjusted to reach pH values of 2.5, 3.5, 4 and 5.5).

126 All the materials and chemicals were sterilized prior to use for the experiments. The abiotic
127 experimental conditions were selected based on preliminary results yielded by biotic
128 experiments in order to compare them as precisely as possible (Balland et al., 2010).

129

130 **2.1. Minerals**

131 The natural 2:1 phyllosilicate used in this study is phlogopite (from
132 Madagascar-Vohitrosy). The chemical composition of this mineral is defined as follows
133 (g/kg): SiO₂ 390; Al₂O₃ 150; Fe₂O₃ 52; MnO 0.9; CaO 2.5; MgO 294; K₂O 110; TiO₂ 11.3;
134 Na₂O 1.3; P₂O₅ 1.1 (Leyval et al., 1990). After undergoing wet grinding and sieving,
135 phlogopite minerals were rinsed under sonication with distilled water at an approximately

136 neutral pH to remove ultrafine particles. The 50-100 μm size fractions of phlogopite were
137 used to conduct experiments. A specific surface area of $0.5 (\pm 0.3) \text{ m}^2 \cdot \text{g}^{-1}$ was determined
138 using the Brunauer-Emmet-Teller N_2 adsorption method. Prior to starting experiments,
139 mineral powders were sterilized at 170°C for 2 hours under dry atmosphere conditions.

140

141 **2.2. Bacterial strains and cultivation**

142 Soil bacteria were preselected based on their contrasting weathering abilities, which
143 represent two main processes: (1) proton-promoted dissolution by “acidifying” bacteria by
144 producing acids such as lactic or acetic acids that do not chelate metals and (2) ligand-
145 promoted dissolution through the production of low molecular mass organic acids that also
146 acidify the medium and chelate metals. Three heterotrophic strains of bacteria (*PAI*, *ARI*,
147 *RAI*) were previously isolated from the rhizospheres of beech, pine and wheat. A
148 complementary strain (*PS2*) was isolated from an acidic soil, i.e., a podzol (WRB) located in
149 the Vosges Mountains in northeastern France (Balland et al., 2010; Djihad Oulkadi et al.,
150 2014). *ARI* and *PS2* dissolve minerals by acidifying the medium, whereas *RAI* and *PAI*
151 produce organic acids (Balland et al., 2010; Leyval and Berthelin, 1991; Djihad Oulkadi et
152 al., 2014).

153 The genus of each bacterial strain was determined by amplifying and sequencing 16S
154 rRNA genes. Polymerase chain reactions were performed using a universal set of primers in a
155 total reaction volume of $50 \mu\text{l}$ containing 1x PCR mastermix (Eppendorf ®), $0.1 \mu\text{M}$ of
156 primers (966 F and 1401 F) and $1 \mu\text{l}$ of cell extract (Fleske 1998). Prior to being sequenced by
157 the MWG Biotech Company (Courtaboeuf, France), the PCR products (PCR product size:
158 433 base pairs) were purified and concentrated using mini-columns (High Pure™ PCR
159 Product Purification Kit, Roche diagnostic). A blast program was then used to compare the
160 sequences with those of the GenBank databases (www.ncbi.nlm.nih.gov/blast). The

161 following identifications were made, with a maximum identification of approximately 99 %:
162 *Rhanella aquatilis* (RA1) and *Pantoea agglomerans* (PA1), which are both anaerobic
163 facultative bacteria, and *Agrobacterium radiobacter* (AR1) and *Pseudomonas sp.* (PS2),
164 which are both aerobic bacteria.

165 All bacterial strains were cryopreserved at -80°C in 30 % glycerol and then
166 precultivated on Petri dishes containing Luna and Bertani agar (LB 20 g.l⁻¹ from Difco and 15
167 g.l⁻¹ agar). Strains were grown at 28°C. Biotic experiments were conducted using an actively
168 growing culture of bacteria that was freshly rinsed and conditioned as described below. Prior
169 to their deposition in the batch reactors, bacterial isolates were recovered and cultivated in 2
170 ml of LB liquid medium for 1 day. Cells in suspension were rinsed three times in deionized
171 water and then suspended in 10 ml of BHm media in order to obtain 10⁷ cells per ml of
172 suspension.

173

174 **2.3. Experimental setup**

175 All experiments (i.e., biotic, abiotic and chemical leaching (without bacteria)
176 experiments) were performed in batch reactor closed systems. Each batch reactor was
177 presterilized with culture media by autoclaving at 110°C for 30 min.

178

179 *2.3.1. Culture media*

180 In all experiments, the classical mineral medium for bacterial cultures (i.e., a Bushnell-
181 Hass-like medium, BHm) was used as a source of essential mineral nutrients for bacteria in
182 order to simulate the chemical composition of a soil solution. This medium was modified to
183 lack iron and magnesium, and phlogopite particles represented the only source of these two
184 bacterial nutrients. Thus, the composition of the Mg- and Fe-free medium was: 20 mg.l⁻¹ KCl;
185 20 mg.l⁻¹ NaH₂PO₄, 2H₂O; 22.5 mg.l⁻¹ Na₂HPO₄, 2H₂O; 65 mg.l⁻¹ (NH₄)₂SO₄; 100 mg.l⁻¹

186 KNO₃; 20 mg.l⁻¹ CaCl₂ (which was dissolved in distilled deionized water to obtain a relatively
187 low ionic strength (4.5 mM).

188 During the microbial weathering of phyllosilicates, glucose is the sole source of carbon and
189 energy. Glucose solutions (20 g.l⁻¹, 0.8 mM of carbon) were thus prepared using ultrapure
190 deionized water (18 MΩ.cm⁻¹, Elga Purelab), and sterilized by filtration at 0.2 μm. All
191 reactants were chosen according to their purity in order to minimize the contamination of Fe
192 and Mg. Neither Fe nor Mg was detected in the medium or in the glucose solution using
193 inductively coupled plasma atomic emission spectroscopy analysis (ICP AES Jobin-Yvon 238
194 at LIMOS, France), which has a detection limit of 5 ppb.

195

196 2.3.2. *Experimental procedure*

197 In addition to the sterility precautions taken throughout all of the experiments, all laboratory
198 materials were precleaned in diluted HNO₃. Biotic and abiotic experiments were run in batch
199 reactors composed of glass flasks. Four leaching experiments (R1 to R4) were performed
200 using RA1, which represents chelating bacteria. One experiment was performed in the
201 presence of other chelating bacteria for comparison (PA1) (experiment #P1). Two phlogopite
202 leaching experiments were performed using the acidifying strain PS2; these were stopped
203 after either 6 days (B1) or 12 days (B2). Another experiment was performed in the presence
204 of other acidifying bacteria, AR1, for comparison, which was stopped after 12 days
205 (experiment #A1). Reactors were continuously agitated using an automatic shaker
206 (Certomatu, Braun 120 rpm), except in experiments R1, R4, P1, A1, H3 and C2, in which
207 flasks were manually agitated every day for approximately 30 seconds. All experiments
208 were conducted under aerobic conditions at a room temperature of 24°C. Each batch was
209 “closed” with carded cotton and greaseproof paper to allow the circulation of ambient air but
210 to protect against bacterial contamination.

211 For biotic experiments, each reactor was filled with 3 g of phlogopite powder, 10 ml
212 of cell suspension, 80 ml of BHm and 10 ml of glucose solution (with a batch concentration
213 of 2 g.l⁻¹). Cell suspensions were incubated in reactors for a duration of 6 to 12 days.
214 The number of bacterial cells in suspension (OD_{600nm}), the consumption of glucose, the nature
215 and quantities of the metabolites that were released and the concentrations of some major
216 elements measured in the leachates were observed as a function of time (Table 1).

217 Abiotic chemical weathering experiments were performed in the same types of glass
218 flasks that were filled with the same amount of phlogopite (3 g) and the same mineral medium
219 (100 ml). Specific acids were added in order to obtain the chosen pH value and
220 concentrations: four experiments were performed using nitric acid (HNO₃) at various pH
221 values (experiments #H1 to #H4) for 6 days for H1 and H2 and for 9 days for H3 and H4.
222 Four experiments were performed using gluconic acid (experiments #G1 to #G4), which were
223 stopped after 6 days for G1, G2 and G4 and after 9 days for G3. Six experiments were
224 performed using citric acid (experiments #C1 to #C6), which were stopped after 6 days for C2
225 to C6 and after 12 days for C1. The leachates collected from both experiments were then
226 filtered at 0.45 µm and stored at 4°C prior to undergoing chemical and isotopic analyses.

227

228 **2.4. Elemental and physiological analyses**

229 *2.4.1. Determination of pH, glucose content and number of bacterial cells*

230 The pH values of these solutions were determined by adding 10 µl of bromocresol
231 green to 200 µl of filtrate. Bromocresol green (BG) is yellow ($\lambda_{\max} = 440$ nm) in acidic
232 solutions (pH < 3.8) and blue ($\lambda_{\max} = 620$ nm) in more basic solutions (pH > 5.8). The pH of
233 each leaching solution was then determined at two wavelengths that are close to both BG
234 maxima (BESHIR et al., 2007). A microplate reader (SAFAS Xenius FLX) was used to
235 measure the absorbance at these various wavelengths.

236 The consumption of glucose by bacteria was determined by measuring the glucose
237 remaining in the 3 μ l of filtered solution after the addition of 300 μ l of GOD-PAP (enzymatic
238 kit, BioLabo). After 20 min, the glucose concentration was measured at an absorbance of 520
239 nm. The detection limit for glucose concentration was 0.1 ppm.

240 The concentration of planktonic bacteria was typically determined by measuring the
241 absorbance of the cell suspension at a wavelength of 600 nm. A correlation between the
242 number of cells and the absorbance was realized by directly enumerating the number of cells
243 with a Thoma cell under microscopic observation as a function of the optical density at 600
244 nm. For each bacterial strain, an equation was obtained to approximate the number of cells in
245 suspension as a function of optical density (data not shown).

246

247 *2.4.2. Metabolites analyses*

248 The ten organic acids that are most commonly released by bacteria were realized and
249 quantified only in experiments R1, B1 and B2 (Table 1). These organic acids are formic,
250 gluconic, butyric, pyruvic, citric, oxalic, propionic, acetic, succinic, malic, lactic and malonic
251 acids. Measurements of these acids were performed using ion chromatography with
252 conductivity detection (ICS 3000, Dionex Corp.) and an analytical column (AS 11 HC,
253 Dionex corp.). Each sample was eluted using a KOH solution of varying concentration (0.9
254 mM to 60 mM) over time (using a step gradient) with a flow of 1.3 ml/min. The synthetic
255 reference materials used were sodium formate, D-gluconic acid, sodium butyrate, pyruvic
256 acid sodium salt, sodium citrate (tribasic), sodium oxalate, sodium propionate, sodium
257 acetate, succinic acid disodium salt, DL-malic acid disodium salt (from Sigma-Aldrich),
258 sodium-L-lactate and malonic acid disodium salt (from Fluka). The uncertainties were better
259 than 0.5 % for all measured organic acids.

260

261 *2.4.3 Magnesium and Si concentrations*

262 The concentrations of the cations (Mg and Si) released in the solution were analyzed using
263 atomic absorption spectrometry (SAA Perkin Elmer 5000 at SARM-CRPG Nancy, CNRS
264 National Facilities, France) and inductively coupled plasma atomic emission spectroscopy
265 (ICP-AES Jobin-Yvon 238 at LIEC Nancy, France). All solution samples were acidified with
266 HNO₃ prior to their analysis. The detection limit for Mg and Si was 0.05 ppm. The
267 uncertainties obtained using our medium were better than 5 %. Accuracy and reproducibility
268 were controlled by repeated analyses of Mg and Si synthetic reference materials (Spex-
269 Certiprep).

270

271 *2.4.4 Magnesium isotope analyses*

272 Magnesium isotopic compositions were determined for solutions collected from all
273 experiments and the initial phlogopite powder. Samples were purified prior to isotopic
274 analysis to reduce interference and matrix effects (Galy et al., 2001). To purify samples, an
275 aliquot of each experimental solution, containing 50 µg of Mg, was evaporated to dryness in a
276 Teflon cup. The residue was then dissolved in a mixture of concentrated nitric acid (HNO₃)
277 and hydrogen peroxide (H₂O₂, 30 %) (4-2 ml) at 80°C overnight to eliminate glucose. The
278 phlogopite sample was dissolved in a mixture of concentrated acid (HNO₃-HF, 3-1 ml) for 48
279 h at 80°C. The mixtures were then evaporated to dryness. All obtained residues were
280 dissolved in 1 ml of 7M HCl, and a few grains of boric acid were added to the solution of
281 phlogopite to avoid any Mg isotope fractionation during this step because the reaction
282 between HF and silicate produces a milky suspension. This is composed of fluoride of
283 calcium and magnesium, together with some mixed fluorides. Boric acid added to digested
284 solution to allow obtaining clear solution and formed the water-soluble fluoroborates (Potts,
285 1987; Zeev and Chien, 1991). The method used to separate Mg from all other elements in this
286 study is described in detail by Bolou-Bi et al., 2009. Purified Mg samples were obtained using

287 three steps of ion-exchange chromatography using a combination of AGMP1-X8 and
288 AG50W-X12 resins.

289 The final purified Mg solutions were evaporated to dryness. The dry samples were
290 diluted with 0.05N HNO₃ at 250 ppb before being introduced into the *Nu Instruments* MC
291 ICP-MS, which is located at the "*Ecole Normale Supérieure*" (National Facilities, ENS-Lyon,
292 France). Magnesium isotopic ratios were measured and normalized relative to the DSM3
293 standard solution (Galy et al., 2001), using a standard-sample bracketing technique to correct
294 for instrumental mass bias. These data are expressed in δ notation to reflect their deviation
295 from the DSM3 composition in parts per thousand (‰):

$$296 \quad \delta^x\text{Mg}(\text{‰}) = \left(\frac{\left(\frac{{}^x\text{Mg}}{{}^{24}\text{Mg}} \right)_{\text{Sample}}}{\left(\frac{{}^x\text{Mg}}{{}^{24}\text{Mg}} \right)_{\text{DSM3}}} - 1 \right) \times 10^3$$

297 where x is either the mass of 26 or 25. The Cambridge-1 pure Mg standard was repeatedly
298 measured during the analytical period and yielded a value of $-2.62\text{‰} \pm 0.13$ (2SD, $n = 3$),
299 which is similar to the overall value of the Cambridge Mg standard in the literature ($-$
300 $2.63\text{‰} \pm 0.11$, $n=1425$, compiled from the literature). Moreover, during Mg isotope
301 purification, a seawater standard (BCR 403) was treated as a sample; it yielded a $\delta^{26}\text{Mg}$ value
302 of $-0.81\text{‰} \pm 0.03$ (2SD, $n = 4$), which is similar to the $\delta^{26}\text{Mg}$ values of seawater that have been
303 reported in the literature ($-0.83\text{‰} \pm 0.11$, $n > 200$; (Ling et al., 2011)).

304

305 **3. RESULTS**

306

307 **3.1 Bacterial growth, glucose consumption and pH variations**

308 The concentration of planktonic bacteria measured during these experiments is given
309 by the optical density measured at 600 nm (OD_{600nm}) (Figure 1a, Table 1, 2). Immediately

310 after inoculation, all reactors with bacteria showed an initial OD_{600nm} value of 0.05, which
311 corresponds to a cell number of $\approx 10^6$ bacteria. ml^{-1} . In experiments using the chelating RA1
312 bacterial strain, cell numbers increased regularly to maximum OD values ranging from 0.21
313 ($\sim 5 \cdot 10^7$ bacteria. ml^{-1}) for experiment R1 to 0.1 ($\approx 10^7$ bacteria. ml^{-1}) for experiment R4. In
314 experiment R3, the maximum OD value was reached at day 3, which then slightly decreased
315 to 0.12 ($1 \cdot 10^7$ bacteria. ml^{-1}). In the presence of the PS2 bacterial strain, cell numbers
316 increased only slightly over time, as the OD values of experiments B1 and B2 reached
317 maximum variations of 0.06 ($\approx 10^6$ bacteria. ml^{-1}) and 0.08 ($5 \cdot 10^6$ bacteria. ml^{-1}), respectively,
318 by the end of their experiments. The acidifying PS2 bacterial strain displayed a different
319 behavior: its cell growth rate remained weak and relatively constant as a function of time (Fig
320 1a).

321 In all biotic reactors, the glucose concentrations strongly decreased after day 0. In the
322 presence of the chelating RA1 bacterial strain, glucose concentrations decreased as a function
323 of time, from 2 $g \cdot l^{-1}$ to 1.02 $g \cdot l^{-1}$ and 1.07 $g \cdot l^{-1}$ for experiments R3 and R4, respectively, on the
324 6th day (Table 2, Figure 1b). In experiment R1, glucose disappeared after day 6.

325 In the presence of the acidifying PS2 strain, glucose concentrations also decreased as a
326 function of time, reaching values of less than 1 $g \cdot l^{-1}$ within the two first days, thus indicating
327 that PS2 consumed more glucose than RA1 at the beginning of these experiments, despite its
328 lower growth rates. The concentrations of glucose then decreased more slightly down to 0.42
329 $g \cdot l^{-1}$ and 0.29 $g \cdot l^{-1}$ for experiments B1 and B2, respectively, after the 6th day. For chelating
330 bacteria, the consumption of glucose and the increase in the number of cells in the solution
331 were interpreted to reflect bacterial growth followed by a prolonged stationary phase that was
332 most likely sustained by the internal recycling of organic matter and nutrients.

333 In all biotic reactors, the pH rapidly decreased within the two first days from an initial
334 value of 6.5 (Figure 1c). On the second day, the pH reached values of 5.2, 5.0, 4.6 and 4.2 for

335 experiments R1, R2, R3 and R4, respectively, in the presence of the chelating bacteria RA1.
336 For experiments with the acidifying bacteria PS2, the pH decreased to lower values of 3.5 and
337 3.3 for experiments B1 and B2, respectively. In all biotic experiments, between days 2 and 12,
338 the pH remained constant except in experiment R1, where the pH again increased on the third
339 day and remained at a relatively constant value of 6.5-6.7. This is linked to the almost
340 complete consumption of glucose by bacteria in this specific experiment. In experiments P1
341 and AR1, the pH values after 12 days were 3.9 and 4.5, respectively. These results are directly
342 linked to glucose consumption and acidification, which are dependent on bacterial
343 metabolism. In our experiments, bacteria used glucose as both an energy source (i.e., electron
344 donor) and a carbon source for biomass synthesis.

345 The decrease in pH observed at the onset of these experiments is likely due to the release of
346 CO₂ by bacteria during respiration and/or the production of organic acids. Low pH values are
347 then maintained by viable bacteria, which release protons, organic acids and CO₂ into solution
348 (Vandevivere et al., 1994; Welch and Ullman, 1999). As shown in the R1 experiment, in the
349 absence of glucose, the decreasing number of bacteria cannot maintain the production of
350 protons and other organic acids. As a consequence, the pH increases due to the consumption
351 of H⁺ that is produced by the chemical alteration of phlogopite. Thus, these data show that
352 both the bacterial growth rate and the mineral alteration rate can affect the chemistry of
353 leachate solutions, as the excretion rate of protons and organic acids is balanced by the release
354 rate of soluble elements from the weathering of phlogopite grains.

355

356 **3.2 Organic acids released by bacteria**

357 In all experiments, the abundances of propionic, malic and malonic acids were below
358 detection limits. In the experiments performed with the chelating RA1 bacterial strain (#R1),
359 the maximum concentrations were reached between the second and third days for lactic acid

360 (62 ppm), acetic acid (152 ppm), formic acid (16.8 ppm), succinic acid (23.5 ppm), oxalic
361 acid (7.2 ppm) and citric acid (3.1 ppm). Between days 2 and 6, the concentrations of organic
362 acids decreased slightly down to 37.1, 0, 8.3, 4.2 and 5.4 ppm for lactic, acetic, formic,
363 succinic and oxalic acids, respectively. A few ppm of citric acid (3.1 ppm) were detected only
364 on the first day. The bacterial strain PS2 (#B2) produced only gluconic and butyric acids. The
365 concentrations of gluconic acid increased from 1600 ppm on day 2 to 2360 ppm on day 6 and
366 2486 ppm on day 12. The concentrations of butyric acid increased from 21 ppm on day 2 to
367 reach 31 ppm on day 6 day and 54 ppm on day 12.

368 The production of organic acids depends on many factors, such as the nutritional,
369 physiological and growth conditions of cultures. Previous studies have shown that the partial
370 oxidation of glucose can lower the pH due to the production of gluconic acid by bacteria
371 (Balland-Bolou-Bi and Poszwa, 2012; Vandevivere et al., 1994; Welch and Ullman, 1999;
372 Wu et al., 2008). In the presence of RA1, the organic acids that were produced included citric
373 and oxalic acids and especially lactic, formic and acetic acids. In contrast, the only major
374 organic acid produced by the acidifying PS2 aerobic bacteria was gluconic acid, which is
375 consistent with its known behavior in natural and laboratory settings (Grybos et al., 2011;
376 Welch and Ullman, 1999). During experiment R1, which was performed with the RA1 strain,
377 glucose was quickly and entirely consumed after 3 days. At the end of day 3, due to the lack
378 of a carbon source, bacterial activity strongly decreased and then stopped. The pH of the
379 solution quickly increased to 7 due to the consumption of protons by the buffering capacity of
380 the phlogopite grains being weathered.

381

382 **3.3 Mg and Si contents in the leachates**

383 The fractions of Mg and Si (F_{Mg} and F_{Si}) leached from phlogopite during the biotic
384 and abiotic experiments were determined and are presented in Table 1 and Fig. 3,

385 respectively. Overall, the Mg and Si fractions are very low for all experiments, both biotic and
386 abiotic, which primarily reflects low weathering rates at these temperatures (24°C). In all
387 cases, F_{Mg} progressively increased as a function of time (Fig. 3) and stabilized after
388 approximately 6 days.

389 Under abiotic conditions, in the experiments performed with HNO_3 (Figure 3B), the dissolved
390 fraction of Mg from phlogopite (F_{Mg}) increased as a function of time and acidity to reach the
391 following values by the end of these experiments: 1.20‰ (H1, day 6); 0.81‰ (H4, day 21)
392 and 0.20‰ (H2, day 6), which occurred at pH values of 2.5, 3.5 and 4.0, respectively. After 6
393 days, the experiments with the lowest pH caused more Mg to be released from phlogopite. In
394 the experiments performed with gluconic acid (Figure 3A), the fractions of dissolved Mg also
395 increased over time and reached values of 0.56‰ (G3, day 9) and 0.25‰ (G4, day 6) at pH
396 values of \approx 3.5 and 4.5, respectively. In the experiments performed with citric acid, the
397 dissolved fraction of Mg from phlogopite (F_{Mg}) increased as a function of time and acidity to
398 reach the following values at the end of these experiments: 0.85‰ (C4, day 12); 0.23‰ (C3,
399 day 6) and 0.50‰ (C4, day 6) at pH values of 5.7, 5.7 and 3.6, respectively. (Fig. 3A).
400 Increases in F_{Mg} with decreases in pH were observed in the experiments performed using
401 HNO_3 and citric and gluconic acids. At an acidic pH (3.5) on day 6, the $f(Mg)$ values of
402 solutions are very close for all experiments (HNO_3 , gluconic and citric acids). These results
403 indicate that gluconic and citric acids act as strong acids at a pH of 3.5, similar to nitric acid.
404 Indeed, the pKa value of gluconic acid is 3.86, whereas those of citric acids are 3.13, 4.76,
405 and 6.4; this indicates that their carboxylic functions are completely dissociated.

406 At a neutral pH (5-6) on day 6, the solutions from the citric acid experiments displayed three
407 times more F_{Mg} than those observed in the HNO_3 experiments, thus reflecting the
408 “complexing effect” of citric acid. Similar to the dissolved Mg fractions in the leachates, the
409 dissolved Si fractions (Table 2) (1) increased over time, (2) increased with decreasing pH in

410 all experiments and (3) exhibited no variations in F_{Si} between treatments on day 6 in low-pH
411 vs high-pH solutions.

412 Under biotic conditions (Fig. 3C), F_{Mg} increased slightly over time in all treatments. In the
413 experiments performed using the RA1, PA1, AR1 strains, F_{Mg} reached 0.6‰ (R3, day 13),
414 0.75‰ (P1, day 12) and 0.56‰ (A1, day 12) with decreases in pH to values of 4.5, 3.9 and
415 4.6, respectively. In experiments performed using the PS2 strain (in which the pH decreased
416 to 3.5), F_{Mg} reached 0.70‰ (B1, day 6) and 1.25‰ (B2, day 12). As observed in abiotic
417 experiments, the dissolved Mg fractions increased when the pH of the leachates decreased.
418 The dissolved Si fractions (F_{Si} ; Table 1) followed the same trend as F_{Mg} in the leachates. In
419 addition, comparing bioleaching and chemical leaching experiments at similar pH values
420 revealed that F_{Mg} was greater in the presence of bacteria or citric acid than in the presence of
421 nitric and gluconic acids.

422

423 **3.5 Mg isotopic signatures**

424 The magnesium measured in the leachates comes exclusively from the weathering of
425 the phlogopite grains introduced in the reactors because all of the nutritive solutions used in
426 the experiments were Mg-free. Magnesium isotopic compositions were measured for 10
427 aliquots of phlogopite grains and the solutions of all experiments (see Tables 1 and 2).

428 The average $\delta^{26}Mg$ value obtained for the phlogopite grains is $-1.22 \pm 0.08\text{‰}$ ($n = 10$). The
429 $\delta^{26}Mg$ values of the solutions range from $-1.52 \pm 0.06\text{‰}$ to $+0.82 \pm 0.02\text{‰}$. Overall, the Mg
430 isotopic compositions of the leachates produced during the bio- and chemical experiments are
431 very close to those of phlogopite. However, two different tendencies as a function of the
432 dissolved Mg fraction can be highlighted. First, the acidifying bacterial strains release the
433 highest Mg fractions to the solution, and their corresponding $\delta^{26}Mg$ values are slightly heavier
434 than those of the initial phlogopite particles (with $\Delta^{26}Mg_{\text{solution-phlogopite}} = +0.13$ to

435 +0.40‰). In contrast, organic acids (except gluconic acid) and the chelating bacteria strains
436 R1, P1 and A1 release lower amounts of Mg to the solution, and their corresponding $\delta^{26}\text{Mg}$
437 values are slightly lighter than those of the phlogopite grains (with $\Delta^{26}\text{Mg} = -0.01$ to -0.30‰).
438 ~~Interestingly,~~ The measurement uncertainties ($\pm 0.10\text{‰}$) are similar to those of lixivate
439 solutions (with an average $\Delta^{26}\text{Mg}$ value of -0.16‰ for ryegrass and clover) produced during
440 phlogopite weathering by plants (Bolou-Bi et al., 2010). Solutions derived from gluconic acid
441 dissolution experiments contain very low Mg, but their $\delta^{26}\text{Mg}$ values are very slightly higher
442 than those of the initial phlogopite particles (with $\Delta^{26}\text{Mg}$ values of up to 0.20‰).

443

444

445 **4. DISCUSSION**

446 **4.1 Assessing congruency and weathering rates**

447 The ratios of the elements released (Mg and Si), together with the elemental ratios of
448 the initial phlogopite as a function of time, are illustrated in Figure 4 and Table 1.

449 *4.1.1. Abiotic experiments*

450 At pH values of 2.5 and 3.5 for experiments H1 and H4 performed by nitric acid,
451 respectively, Mg/Si decreased slightly with increasing pH (to 0.98, 0.92 and 0.92 at pH values
452 of 2.5, 3.5 and 4, respectively, at 6 days). However, they are similar to the bulk initial ratio of
453 the phlogopite (0.97). These values of Mg/Si are in good agreement with those obtained by
454 Kalinowski and Schweda, 1996 during the dissolution of phlogopite by HNO_3 .

455 In our study, during abiotic leaching in the presence of citric acid (experiments C3 and C4),
456 the Mg/Si ratios (0.95 and 0.7, respectively) were slightly lower than the Mg/Si ratio of the
457 phlogopite (0.97), thus indicating that in contrast to the observation of Barman et al., 1992, Si
458 was preferentially released. At a pH of 3.5, the preferential elemental release that occurred
459 was $\text{Fe} > \text{Al} > \text{Mg} = \text{Si}$, with $F_{\text{Fe}} = 2.02$; $F_{\text{Al}} = 1.82$; $F_{\text{Mg}} = 0.53$ and $F_{\text{Si}} = 0.56\text{‰}$. The

460 difference between our results and those of Barman et al., 1992 can be explained by the fact
461 that at a pH of 3.5, only two carboxylic groups of citric acid were dissociated (pKa= 3.13;
462 4.76; 6.4); it is known that citrates have a strong affinity for iron to the detriment of
463 magnesium, in comparison to their experiments, where citric acid caused all of these
464 carboxylic groups to dissociate. Nevertheless, the high concentrations of citric acid (1 mM)
465 used in our chemical experiments do not reflect their concentrations in bioleaching
466 experiments in the presence of RA1 (approximately 3 ppm or 0.02 mM). High concentrations
467 of organic acids can enhance surface complexation processes, which can decrease the number
468 of surface reactive sites and consequently lead to a saturation of rates (Golubev et al., 2006).
469 These observations were confirmed by experiments C5 and C6, which were performed with
470 high concentrations of citric acid (10 to 100 mM) that led to Mg/Si ratios in solution that were
471 significantly lower (approximately 0.56) than those in experiment C3 (0.95), but with a
472 similar Mg value of 1.5 ppm after 6 days.

473 *4.1.2. Biotic experiments*

474 All other experiments (bio- and chemical leaching) yielded Mg/Si values that were
475 less than the bulk initial ratio of the phlogopite, except for the experiments performed with the
476 chelating bacterial strain RA1 (which yielded a Mg/Si value of approximately 1.5). In the
477 presence of RA1 (experiments R2 and R3), Mg was preferentially released compared to Si.
478 This reflects the greater dissolution of octahedra compared with tetrahedra. Acker and
479 Bricker, 1992 demonstrated that at a pH of greater than 3 (in the case of our experiments R1
480 to R4, which had pH values of close to 4.5), biotite octahedra were preferentially destroyed.
481 Moreover, Barman et al., 1992 highlighted that biotite weathering in the presence of a strong
482 chelating agent, such as citric or oxalic acid, preferentially released Mg into solution over Si;
483 this was the case in our experiment R1, where low amounts of oxalic and citric acids were
484 quantified (approximately 7 and 3 ppm for oxalic and citric acids, respectively). The results of

485 Barman et al. (1992) indicated that chemical leaching in the presence of citric acid
486 preferentially releases Mg compared to Si due to the high solubility of Mg and that the
487 localization of Mg in octahedra makes Mg easily accessible to the solution. At a pH of 1, the
488 authors demonstrated that preferential elemental release occurred in the following order: Mg >
489 Fe > Al > Si.

490 In the experiments performed with the bacterial strain PS2 (B2) and gluconic acid (G4), the
491 Mg/Si ratios were very close to the bulk ratio of phlogopite (0.97) and those obtained in the
492 experiment performed with HNO₃ (H4). This observation is consistent with the results of the
493 Mg and Si release rates, which indicate that pH exerts a control on the leaching of Mg and Si
494 from phlogopite, as well as the results of several works (Grybos et al., 2011; Oulkadi et al.,
495 2014b), which showed that *Pseudomonas* sp. can weather clay from both octahedral and
496 tetrahedral layers. As mentioned above, at this acidic pH, gluconic acid acts similar to a
497 mineral acid, such as nitric acid.

498 These different types of bacteria may play different roles in the dissolution rate of
499 phlogopite and can therefore have different influences on the chemical composition of the
500 solutions. To remind, *AR1 and PS2* dissolve minerals by acidifying the medium, whereas *RA1*
501 and *PA1* produce organic acids (Balland et al., 2010; Leyval and Berthelin, 1991; Djihad
502 Oulkadi et al., 2014). Thus, for the facultative anaerobic bacteria (*RA1* and *PA1*), under
503 conditions of stress, the glucose oxidation continued beyond the glucose intermediate. The
504 lack of required enzymes caused some bacteria to accumulate or expel various intermediate
505 acids as waste (Gottschalk, 1986), such as fumaric, citric, and oxalic acids and especially
506 lactic, pyruvic and acetic acids resulting from fermentation. Thus, these strains have an
507 anabolism that requires little energy. Consequently, their catabolism is not very efficient, as it
508 uses a small fraction of the initial carbon in the solution (i.e., glucose). In contrast, the *PS2*
509 strain is an aerobic bacterial strain that has an anabolism that requires more energy and an

510 efficient catabolism that requires large amounts of carbon. Moreover, D. Oulkadi et al., 2014a
511 showed that RA1 produces siderophores, whereas PS2 does not. Siderophores and oxalic and
512 citric acids clearly displayed ligand-promoted dissolution in addition to proton-promoted
513 dissolution.

514 4.1.3. Weathering rates

515 To more precisely assess the controls of Mg and Si release and compare them with published
516 estimates, their concentrations were normalized to the specific surface area of phlogopite and
517 time (r_{Mg} and r_{Si} are both expressed in $\text{mol}\cdot\text{m}^{-2}\cdot\text{s}^{-1}$). The influence of pH, organic acids and
518 bacteria on the release rates of Mg and Si could therefore be evaluated using the linear rate
519 law described by Malmström and Banwart, (1997) and Malmström et al., (1996), which is
520 given by the following equation:

$$521 \quad r_M = k_H (a_{H^+})^n + k_O + k_{OH} (a_{OH})^m + k_{L,M} (a_L)^l \text{ (eq. 1)}$$

522 where M is the released element (Mg or Si); k is the rate constant; a_{H^+} , a_{OH} and a_L are the
523 activities of protons, hydroxyls and ligands, respectively; and n, m, and l are the orders of
524 reactions that are experimentally obtained with respect to protons, hydroxyls and ligands,
525 respectively. This model assumes that (1) ligand-promoted processes operate in parallel with
526 and independently of hydroxyl- or proton-promoted processes, and (2) ligand-promoted rates
527 are additive. In this study, because phlogopite weathering occurs in an acidic environment, the
528 terms k_O and $k_{OH} (a_{OH})^m$ are negligible. Thus, experimental data can be fitted to the rate law to
529 yield the following equation:

$$530 \quad r_M = k_H (a_{H^+})^n + k_{L,M} (a_L)^l \text{ (eq. 2)}$$

531 The form of this empirical release rate equation is characteristic of dissolution rate laws in
532 which proton adsorption or ligand complexation occurs at the mineral surface. For phlogopite,
533 the apparent dissolution rate constant, which is normalized to the surface area, is $K_H = 4.7 \cdot 10^{-9}$
534 $\text{mol}\cdot\text{m}^{-2}\cdot\text{s}^{-1}$. The reaction order (n) with respect to hydrogen ion activity is 0.42, which is in

535 good agreement with the values provided in the literature (Balland et al., 2010; Kalinowski
536 and Schweda, 1996; Rufe and Hochella, 1999; Taylor et al., 2000).

537 In both biotic and abiotic experiments, the apparent initial release rates of Mg and Si were
538 calculated using equation 2. In all experiments, the release rates of Mg and Si decreased
539 slightly with time. This has frequently been observed in dissolution experiments using fresh
540 mineral samples, as in the works of Furrer and Stumm, (1986) and Malmström and Banwart
541 (1997). This could be attributed to the initial rapid dissolution of ultrafine particles, which is
542 then followed by a decrease in the dissolving surface area and the creation of more reactive
543 surface sites.

544 Figure 4 represents the Mg (r_{Mg}) and Si (r_{Si}) release rates as functions of average pH.
545 The observed correlations confirmed that this elemental release was largely pH-controlled.
546 The highest elemental release rates occurred at low pH values, whereas the lowest rates
547 occurred at nearly neutral pH values.

548 It can also be observed that biotic and abiotic experiments performed with citric acid or with
549 produced citric acid have higher release rates relative to abiotic experiments performed with
550 HNO₃ and gluconic acid. At a given pH, Mg release rates were ~ 2 to 3 times higher in the
551 presence of bacteria compared to those observed during chemical leaching performed with
552 HNO₃. Silicon release rates were also ~ 1.5 times higher in the presence of bacteria. The
553 organic acids released by bacteria play an important role in the release of Si. Acidifying
554 bacteria (PS2 and AR1) amplified Mg and Si release rates compared to HNO₃. As shown in
555 the organic acid analyses, the PS2 strain produced approximately 1 mM of gluconic acid into
556 solution, leading to a pH of 3.5. At this pH, Mg and Si release rates were lower and similar to
557 those observed during chemical experiments performed only with gluconic acid (G1, G2 and
558 G3 ~ $1.43 \cdot 10^{-10}$ mol.m⁻².s⁻¹) and HNO₃ (H4) ($1.38 \cdot 10^{-10}$ mol.m⁻².s⁻¹). Moreover, at this pH,
559 gluconic acid (pK_a = 3.86) acted as a strong acid. However, the enhanced elemental release

560 rates in the presence of PS2 and AR1 suggest that other processes must be taken into account
561 to interpret such variations. Vandevivere et al., (1994) highlighted microreaction zones at the
562 bacteria-mineral contact where the chemical compositions of the solution in these sites were
563 strongly different compared to that of the bulk solution, with high concentrations of protons
564 and organic acids.

565 All of the bacterial strains used in this work, including both acidifying (PS2 and AR1) and
566 chelating (PA1 and RA1) bacteria, principally accelerate the release of elements (Mg and Si)
567 from phlogopite by decreasing the solution pH and/or producing chelating agents, such as
568 organic acids. Similar conclusions have previously been reported (Barker et al., 1998;
569 Vandevivere et al., 1994; Wu et al., 2008). Thus, it seems that the production of organic acids
570 and siderophores plays a crucial role in the mechanism and efficiency of clay dissolution.
571 Several studies (Cheah et al., 2003; D. Oulkadi et al., 2014b; Reichard et al., 2007) have
572 demonstrated that the presence of siderophores could be strongly affected by the presence of
573 oxalic acid inducing the high dissolution of minerals.

574 The measured growth of bacteria was not correlated to the Mg and Si released into solution
575 during the bioleaching of phlogopite. This suggests that the growth of bacteria was not a
576 crucial factor in highlighting the effectiveness of bacteria to weather phlogopite, as indicated
577 by the relationship between the cell numbers and the elemental release rate. Indeed, the cell
578 number of PS2 was less important than that of RA1, while elemental release was more
579 important in the presence of the PS2 bacterial strain ($2.22 \cdot 10^{-10}$ and $2.51 \cdot 10^{-10}$ mol.m⁻².s⁻¹ for
580 Mg and Si release rates, respectively) than in the presence of the RA1 bacterial strain
581 ($1.06 \cdot 10^{-10}$ and $7.23 \cdot 10^{-11}$ mol.m⁻².s⁻¹). However, only planktonic bacteria were enumerated in
582 our experiments, whereas adhering bacteria are known to play an important role in enhancing
583 mineral weathering (Vandevivere et al., 1994). At this stage of our study, it is not possible to
584 determine the number of bacteria cells that were adsorbed onto phlogopite particles.

585

586 **4.2 Magnesium isotope variations**

587 The low dissolution rate associated with the low Mg fraction released during the
588 dissolution experiment could be the reason of similar $\delta^{26}\text{Mg}$ values of the solution and initial
589 phlogopite in the measurement uncertainties. This similarly $\delta^{26}\text{Mg}$ values suggests that no
590 fractionation occurred during the acid congruent dissolution of phlogopite under these
591 conditions in the measurement uncertainties. Although the $\delta^{26}\text{Mg}$ values of solutions are close
592 to the $\delta^{26}\text{Mg}$ value of phlogopite, two tendencies can be distinguished (Fig. 6).

593 Results indicate that more Mg is released in solution; more $\delta^{26}\text{Mg}$ value of the
594 solution is heavier compared to initial phlogopite (Fig 6), and *vice versa*. These $\delta^{26}\text{Mg}$ values
595 are strongly correlated to solution pH (Fig 7), which suggests at first approximation that the
596 mode of medium acidification (i.e., proton-promoted *vs* ligand-promoted agent used to leach
597 Mg from a mineral) could explain the various $\delta^{26}\text{Mg}$ values observed in solutions
598 independently of the vital effect.

599 During phlogopite leaching by ligand-promoted dissolution, the decrease in the solution pH is
600 associated with a light $\delta^{26}\text{Mg}$ value compared to fresh phlogopite. In contrast, during
601 phlogopite leaching by proton-promoted dissolution (i.e., nitric acid and *Pseudomonas*
602 bacterial strain), the decrease in the solution pH is associated with a heavy $\delta^{26}\text{Mg}$ value
603 compared to fresh phlogopite. These results are in agreement with results found during clay
604 mineral formation (Wimpenny et al., 2014). In soil clay, some Mg can be bound to functional
605 groups on the clay surface as exchangeable Mg in addition to existing as a structural part of
606 the octahedral layer (Drever, 1988; Opfergelt et al., 2012; Wimpenny et al., 2014). According
607 to the classification of trioctahedral mica, we could assume based on studies of cation
608 exchange capacity that Mg in phlogopite derived from both structural site located in the
609 octahedral layer and on exchangeable site at the mineral surface. Exchangeable Mg is

610 isotopically lighter than clay in soil and bulk soil (Bolou-Bi et al., 2012; Opfergelt et al.,
611 2012; Uhlig et al., 2017). In addition, the leaching of the exchangeable Mg on clay with
612 organic acids shown that this fraction is isotopically lighter than clay (Wimpenny et al.,
613 2014), similarly to results found during the ligand-promoted experiment in this study (Table
614 1). The use of strong acid would induce the leaching of both exchangeable Mg and structural
615 Mg during the experiment. During proton-promoted dissolution, the $\delta^{26}\text{Mg}$ value of Mg
616 released into solution increased with the increasing mineral dissolution rate, in contrast to
617 experiments with ligand-promoted dissolution (Fig. 6), except those performed with gluconic
618 acid, which acts as a mineral acid under these conditions. Magnesium located in structural
619 sites is contained in the brucitic layer. The leaching of this structural Mg is associated with
620 the release of other ions located in this octahedral layer, such as Al. Moreover, in these
621 minerals, Si is located in polymerized sheets of silica tetrahedral. The release of Si in solution
622 reflects the dissolution of this structure in addition to the octahedral layer, as indicated by the
623 correlation between Si and Mg (Fig. 4). Various Mg isotopic analyses during the synthesis of
624 brucite demonstrate that it is enriched in heavy isotope in comparison with the solution (Li et
625 al., 2014; Wimpenny et al., 2014). Therefore, we could conceive that Mg leaching in the
626 structural sites using a strong acid (proton) would be the origin of heavy Mg isotopes
627 enrichment in solutions.

628 The fractionation of Mg isotopes by bacteria is a complex process especially since it is
629 dependent on the bacterium studied. Our work has highlighted the non-negligible role of
630 bacterial metabolism (through the production of organic acids) during silicate weathering at
631 ambient temperature in batch reactor. Additional experiments are needed to increase the Mg
632 leaching from phlogopite by increasing time reaction in order to measure Mg uptake by
633 bacteria (and if there is some Mg isotopes fractionation during this process) and analyze the
634 Mg isotopic ratio in the reacted phlogopite in order to see if there is a formation of secondary

635 phase. Future work should focus on linking Mg isotopic fractionation to these reactions. Mg
636 isotopes appear to be well-suited tools for the discovery of biological markers on Earth.
637 However, a variety of abiotic chemical reactions could play a complicated role.

638

639 4. CONCLUSIONS

640 This study demonstrates that the decreases in pH and metabolites produced during
641 heterotrophic bacterial activities could greatly accelerate the release of Mg and Si from
642 phlogopite. Comparing bioleaching and chemical leaching experiments performed at similar
643 pH values reveals that more elements were released into solution in the presence of bacteria
644 or citric acid compared with those released in the presence of nitric and gluconic acids.
645 Bacterial metabolism differs from one strain to another and induces substantial changes in
646 solution pH; these changes had important effects on the rate of elemental release from
647 phlogopite compared those observed under abiotic conditions. In our experiments, aerobic
648 bacterial strains were more efficient than facultative anaerobe bacteria in leaching Mg during
649 phlogopite weathering.

650 In most experiments, little to no Mg isotopic fractionation linked to phlogopite leaching was
651 highlighted. However, two tendencies could be distinguished, especially in the highest
652 leached Mg fractions obtained: (1) for experiments performed with HNO₃ and the acidifying
653 bacteria PS2, the Mg leached into solution was enriched in its heavy isotope compared to
654 phlogopite; (2) for experiments performed with citric acid, the Mg leached into solution was
655 enriched in its light isotope compared to phlogopite. However, the Mg isotopic fractionation
656 factor was very low, thus indicating that little to no fractionation occurred during our
657 experiments, which correspond to the first event of the bioleaching of phlogopite (in a closed
658 system). Moreover, when high phlogopite dissolution rates are correlated with low pH values,
659 the Mg isotopic composition of the leached solution is enriched in heavy isotopes, which

660 reflects the leaching of structural Mg contained in the octahedra of phlogopite. In experiments
661 performed with chelating bacteria and citric acid, high phlogopite dissolution rates were
662 enriched in light isotopes, especially at weak acid pH (4-6) values, due to the formation of
663 secondary minerals or the leaching of the Mg adsorbed on the minerals.

664

665 **5. ACKNOWLEDGEMENTS**

666 Philippe Telouk for CNRS-INSU facilities and help with isotopic analyses at ENS-Lyon. We
667 are grateful to Editor and Josh Wimpenny for comments to improve this manuscript.
668

669 **6. REFERENCES CITED**

- 670 Acker, J.G., Bricker, O.P., 1992. The influence of pH on biotite dissolution and alteration
671 kinetics at low temperature. *Geochim. Cosmochim. Acta* 56, 3073–3092.
672 doi:10.1016/0016-7037(92)90290-Y
- 673 Anbar, A.D., 2004. Iron stable isotopes: Beyond biosignatures. *Earth Planet. Sci. Lett.* 217,
674 223–236. doi:10.1016/S0012-821X(03)00572-7
- 675 Balland-Bolou-Bi, C., Poszwa, A., 2012. Effect of calco-magnesian amendment on the
676 mineral weathering abilities of bacterial communities in acidic and silicate-rich soils.
677 *Soil Biol. Biochem.* 50, 108–117. doi:10.1016/j.soilbio.2012.02.034
- 678 Balland, C., Poszwa, A., Leyval, C., Mustin, C., 2010. Dissolution rates of phyllosilicates as a
679 function of bacterial metabolic diversity. *Geochim. Cosmochim. Acta* 74, 5478–5493.
680 doi:10.1016/j.gca.2010.06.022
- 681 Barker, W.W., Banfield, J.F., 1998. Zones of chemical and physical interaction at interfaces
682 between microbial communities and minerals: A model. *Geomicrobiol. J.* 15, 223–244.
683 doi:10.1080/01490459809378078
- 684 Barker, W.W., Welch, S.A., Chu, S., Banfield, J.F., 1998. Experimental observations of the
685 effects of bacteria on aluminosilicate weathering. *Am. Mineral.* 83, 1551–1563.
686 doi:10.2138/am-1998-1116
- 687 Barman, A.K., Varadachari, C., Ghosh, K., 1992. Weathering of silicate minerals by organic
688 acids. I. Nature of cation solubilisation. *Geoderma* 53, 45–63. doi:10.1016/0016-
689 7061(92)90020-8
- 690 Bastian, L., Revel, M., Bayon, G., Dufour, A., Vigier, N., 2017. Abrupt response of chemical
691 weathering to Late Quaternary hydroclimate changes in northeast Africa. *Sci. Rep.* 7.
692 doi:10.1038/srep44231
- 693 Beard, B.L., 1999. Iron Isotope Biosignatures. *Science* (80-.). 285, 1889–1892.
694 doi:10.1126/science.285.5435.1889
- 695 Beard, B.L., Johnson, C.M., Skulan, J.L., Nealson, K.H., Cox, L., Sun, H., 2003. Application
696 of Fe isotopes to tracing the geochemical and biological cycling of Fe. *Chem. Geol.* 195,

- 697 87–117. doi:10.1016/S0009-2541(02)00390-X
- 698 Bennett, P.C., Hiebert, F.K., Choi, W.J., 1996. Microbial colonization and weathering of
699 silicates in a petroleum-contaminated groundwater. *Chem. Geol.* 132, 45–53.
700 doi:10.1016/S0009-2541(96)00040-X
- 701 Bennett, P.C., Rogers, J.R., Choi, W.J., 2001. Silicates, silicate weathering, and microbial
702 ecology. *Geomicrobiol. J.* 18, 3–19. doi:10.1080/01490450151079734
- 703 Berner, R.A., 1992. Weathering, plants, and the long-term carbon cycle. *Geochim.*
704 *Cosmochim. Acta* 56, 3225–3231. doi:10.1016/0016-7037(92)90300-8
- 705 Black, J.R., Epstein, E., Rains, W.D., Yin, Q.Z., Casey, W.H., 2008. Magnesium-isotope
706 fractionation during plant growth. *Environ. Sci. Technol.* 42, 7831–7836.
707 doi:10.1021/es8012722
- 708 Bolou-Bi, B.E., Dambrine, E., Angeli, N., Pollier, B., Nys, C., Guerold, F., Legout, A., 2016.
709 Magnesium Isotope Variations to Trace Liming Input to Terrestrial Ecosystems: A Case
710 Study in the Vosges Mountains. *J. Environ. Qual.* 45, 276–84.
711 doi:10.2134/jeq2015.02.0096
- 712 Bolou-Bi, E.B., Poszwa, A., Leyval, C., Vigier, N., 2010. Experimental determination of
713 magnesium isotope fractionation during higher plant growth. *Geochim. Cosmochim.*
714 *Acta* 74, 2523–2537. doi:10.1016/j.gca.2010.02.010
- 715 Bolou-Bi, E.B., Vigier, N., Brenot, A., Poszwa, A., 2009. Magnesium isotope compositions
716 of natural reference materials. *Geostand. Geoanalytical Res.* 33, 95–109.
717 doi:10.1111/j.1751-908X.2009.00884.x
- 718 Bolou-Bi, E.B., Vigier, N., Poszwa, A., Boudot, J.P., Dambrine, E., 2012. Effects of
719 biogeochemical processes on magnesium isotope variations in a forested catchment in
720 the Vosges Mountains (France). *Geochim. Cosmochim. Acta* 87, 341–355.
721 doi:10.1016/j.gca.2012.04.005
- 722 Brantley, S.L., Liermann, L., Bullen, T.D., 2001. Fractionation of Fe isotopes by soil
723 microbes and organic acids. *Geology* 29, 535–538. doi:10.1130/0091-
724 7613(2001)029<0535:FOFIBS>2.0.CO
- 725 Brantley, S.L., Liermann, L.J., Guynn, R.L., Anbar, A., Icopini, G.A., Barling, J., 2004. Fe
726 isotopic fractionation during mineral dissolution with and without bacteria. *Geochim.*
727 *Cosmochim. Acta* 68, 3189–3204. doi:10.1016/j.gca.2004.01.023
- 728 Brenot, A., Cloquet, C., Vigier, N., Carignan, J., France-Lanord, C., 2008. Magnesium
729 isotope systematics of the lithologically varied Moselle river basin, France. *Geochim.*
730 *Cosmochim. Acta* 72, 5070–5089. doi:10.1016/j.gca.2008.07.027
- 731 Cheah, S.F., Kraemer, S.M., Cervini-Silva, J., Sposito, G., 2003. Steady-state dissolution
732 kinetics of goethite in the presence of desferrioxamine B and oxalate ligands:
733 Implications for the microbial acquisition of iron. *Chem. Geol.* 198, 63–75.
734 doi:10.1016/S0009-2541(02)00421-7
- 735 Drever, J.I., 1988. *The Geochemistry of Natural Waters*, 2nd Editio. ed. Prentice-Hall,
736 Englewood Cliffs, 437 p.
- 737 Fahad, Z.A., Bolou-Bi, E.B., Köhler, S.J., Finlay, R.D., Mahmood, S., 2016. Fractionation
738 and assimilation of Mg isotopes by fungi is species dependent. *Environ. Microbiol. Rep.*

- 739 8, 956–965. doi:10.1111/1758-2229.12459
- 740 Furrer, G., Stumm, W., 1986. The coordination chemistry of weathering: I. Dissolution
741 kinetics of $[\delta]\text{-Al}_2\text{O}_3$ and BeO. *Geochim. Cosmochim. Acta* 50, 1847–1860.
742 doi:10.1016/0016-7037(86)90243-7
- 743 Galy, A., Bar-Matthews, M., Halicz, L., O’Nions, R.K., 2002. Mg isotopic composition
744 of carbonate: Insight from speleothem formation. *Earth Planet. Sci. Lett.* 201, 105–115.
745 doi:10.1016/S0012-821X(02)00675-1
- 746 Galy, A., Belshaw, N.S., Halicz, L., O’Nions, R.K., 2001. High-precision measurement of
747 magnesium isotopes by multiple-collector inductively coupled plasma mass
748 spectrometry. *Int. J. Mass Spectrom.* 208, 89–98. doi:10.1016/S1387-3806(01)00380-3
- 749 Golubev, S. V., Bauer, A., Pokrovsky, O.S., 2006. Effect of pH and organic ligands on the
750 kinetics of smectite dissolution at 25 °C. *Geochim. Cosmochim. Acta* 70, 4436–4451.
751 doi:10.1016/j.gca.2006.06.1557
- 752 Gottschalk, G., 1986. *Bacterial metabolism*, Springer-V. ed. New-York.
- 753 Grybos, M., Billard, P., Desobry-Banon, S., Michot, L.J., Lenain, J.F., Mustin, C., 2011. Bio-
754 dissolution of colloidal-size clay minerals entrapped in microporous silica gels. *J.*
755 *Colloid Interface Sci.* 362, 317–324. doi:10.1016/j.jcis.2011.07.031
- 756 Huang, K.J., Teng, F.Z., Wei, G.J., Ma, J.L., Bao, Z.Y., 2012. Adsorption- and desorption-
757 controlled magnesium isotope fractionation during extreme weathering of basalt in
758 Hainan Island, China. *Earth Planet. Sci. Lett.* 359–360, 73–83.
759 doi:10.1016/j.epsl.2012.10.007
- 760 Hutchens, E., Valsami-Jones, E., McEldowney, S., Gaze, W., McLean, J., 2003. The role of
761 heterotrophic bacteria in feldspar dissolution – an experimental approach. *Mineral. Mag.*
762 67, 1157–1170. doi:10.1180/0026461036760155
- 763 Kalinowski, B.E., Schweda, P., 1996. Kinetics of muscovite, phlogopite, and biotite
764 dissolution and alteration at pH 1–4, room temperature. *Geochim. Cosmochim. Acta* 60,
765 367–385. doi:10.1016/0016-7037(95)00411-4
- 766 Leyval, C., Berthelin, J., 1991. Weathering of a Mica by Roots and Rhizospheric
767 Microorganisms of Pine. *Soil Sci. Soc. Am. J.* 55, 1009–1016.
768 doi:10.2136/sssaj1991.03615995005500040020x
- 769 Leyval, C., Laheurte, F., Belgy, G., Berthelin, J., 1990. Weathering of Micas in the
770 Rhizospheres of Maize, Pine and Beech Seedlings Influenced by Mycorrhizal and
771 Bacterial Inoculation. *Symbiosis* 9, 105–109.
- 772 Li, W., Beard, B.L., Li, C., Johnson, C.M., 2014. Magnesium isotope fractionation between
773 brucite $[\text{Mg}(\text{OH})_2]$ and Mg aqueous species: Implications for silicate weathering and
774 biogeochemical processes. *Earth Planet. Sci. Lett.* doi:10.1016/j.epsl.2014.03.022
- 775 Li, W.Y., Teng, F.Z., Ke, S., Rudnick, R.L., Gao, S., Wu, F.Y., Chappell, B.W., 2010.
776 Heterogeneous magnesium isotopic composition of the upper continental crust.
777 *Geochim. Cosmochim. Acta* 74, 6867–6884. doi:10.1016/j.gca.2010.08.030
- 778 Ling, M.X., Sedaghatpour, F., Teng, F.Z., Hays, P.D., Strauss, J., Sun, W., 2011.
779 Homogeneous magnesium isotopic composition of seawater: An excellent geostandard
780 for Mg isotope analysis, in: *Rapid Communications in Mass Spectrometry*. pp. 2828–

- 781 2836. doi:10.1002/rcm.5172
- 782 Liu, S.A., Teng, F.Z., Yang, W., Wu, F.Y., 2011. High-temperature inter-mineral magnesium
783 isotope fractionation in mantle xenoliths from the North China craton. *Earth Planet. Sci.*
784 *Lett.* 308, 131–140. doi:10.1016/j.epsl.2011.05.047
- 785 Maguire, M.E., 2006. Magnesium transporters: properties, regulation and structure. *Front.*
786 *Biosci.* 11, 3149–3163. doi:10.2741/2039
- 787 Malmström, M., Banwart, S., 1997. Biotite dissolution at 25°C: The pH dependence of
788 dissolution rate and stoichiometry. *Geochim. Cosmochim. Acta* 61, 2779–2799.
789 doi:10.1016/S0016-7037(97)00093-8
- 790 Malmström, M., Banwart, S., Lewenhagen, J., Duro, L., Bruno, J., 1996. The dissolution of
791 biotite and chlorite at 25°C in the near-neutral pH region, in: *Journal of Contaminant*
792 *Hydrology*. pp. 201–213. doi:10.1016/0169-7722(95)00047-X
- 793 Maloney, K.E., Valvano, M.A., 2006. The *mgtC* gene of *Burkholderia cenocepacia* is
794 required for growth under magnesium limitation conditions and intracellular survival in
795 macrophages. *Infect. Immun.* 74, 5477–5486. doi:10.1128/IAI.00798-06
- 796 Mathur, R., Ruiz, J., Titley, S., Liermann, L., Buss, H., Brantley, S., 2005. Cu isotopic
797 fractionation in the supergene environment with and without bacteria. *Geochim.*
798 *Cosmochim. Acta* 69, 5233–5246. doi:10.1016/j.gca.2005.06.022
- 799 Mavromatis, V., Pearce, C.R., Shirokova, L.S., Bundeleva, I.A., Pokrovsky, O.S., Benezeth,
800 P., Oelkers, E.H., 2012. Magnesium isotope fractionation during hydrous magnesium
801 carbonate precipitation with and without cyanobacteria. *Geochim. Cosmochim. Acta* 76,
802 161–174. doi:10.1016/j.gca.2011.10.019
- 803 Opfergelt, S., Georg, R.B., Delvaux, B., Burton, K.W., Cabidoche, Y.-M., Halliday, A.N.,
804 2012. Mechanisms of magnesium isotope fractionation in volcanic soil weathering
805 sequences, Guadeloupe. *Earth Planet. Sci. Lett.* 341–344, 176–185.
806 doi:10.1016/j.epsl.2012.06.010
- 807 Oulkadi, D., Balland-Bolou-Bi, C., Billard, P., Kitzinger, G., Parrello, D., Mustin, C., Banon,
808 S., 2014. Interactions of three soil bacteria species with phyllosilicate surfaces in hybrid
809 silica gels. *FEMS Microbiol. Lett.* doi:10.1111/1574-6968.12421
- 810 Oulkadi, D., Balland-Bolou-Bi, C., Billard, P., Kitzinger, G., Parrello, D., Mustin, C., Banon,
811 S., 2014a. Interactions of three soil bacteria species with phyllosilicate surfaces in hybrid
812 silica gels. *FEMS Microbiol. Lett.* 354. doi:10.1111/1574-6968.12421
- 813 Oulkadi, D., Balland-Bolou-Bi, C., Michot, L.J., Grybos, M., Billard, P., Mustin, C., Banon,
814 S., 2014b. Bioweathering of nontronite colloids in hybrid silica gel: Implications for iron
815 mobilization. *J. Appl. Microbiol.* 116, 325–334. doi:10.1111/jam.12361
- 816 Pelmont, J., 1993. *Bactéries et environnement*, Presse uni. ed. Grenoble.
- 817 Pogge von Strandmann, P.A.E., James, R.H., van Calsteren, P., Gíslason, S.R., Burton, K.W.,
818 2008. Lithium, magnesium and uranium isotope behaviour in the estuarine environment
819 of basaltic islands. *Earth Planet. Sci. Lett.* 274, 462–471. doi:10.1016/j.epsl.2008.07.041
- 820 Potts, P.J., 1987. *A Handbook of Silicate Rock Analysis*. Springer Netherlands.
821 doi:10.1007/978-94-015-3988-3
- 822 Reichard, P.U., Kretzschmar, R., Kraemer, S.M., 2007. Dissolution mechanisms of goethite in

- 823 the presence of siderophores and organic acids. *Geochim. Cosmochim. Acta* 71, 5635–
824 5650. doi:10.1016/j.gca.2006.12.022
- 825 Robert, M., Berthelin, J., 1986. Role of biological and Biochemical factors in soil mineral
826 weathering. *Soil Sci. Soc. Am. J.* 12, 453–495.
- 827 Rogers, J.R., Bennett, P.C., 2004. Mineral stimulation of subsurface microorganisms: Release
828 of limiting nutrients from silicates. *Chem. Geol.* 203, 91–108.
829 doi:10.1016/j.chemgeo.2003.09.001
- 830 Rufe, E., Hochella, M., 1999. Quantitative Assessment of Reactive Surface Area of
831 Phlogopite During Acid Dissolution. *Science* (80-.). 285, 874–876.
832 doi:10.1126/science.285.5429.874
- 833 Ryu, J.S., Vigier, N., Decarreau, A., Lee, S.W., Lee, K.S., Song, H., Petit, S., 2016.
834 Experimental investigation of Mg isotope fractionation during mineral dissolution and
835 clay formation. *Chem. Geol.* 445, 135–145. doi:10.1016/j.chemgeo.2016.02.006
- 836 Taylor, A.S., Blum, J.D., Lasaga, A.C., MacInnis, I.N., 2000. Kinetics of dissolution and Sr
837 release during biotite and phlogopite weathering. *Geochim. Cosmochim. Acta* 64, 1191–
838 1208. doi:10.1016/S0016-7037(99)00369-5
- 839 Tipper, E.T., Gaillardet, J., Louvat, P., Capmas, F., White, A.F., 2010. Mg isotope constraints
840 on soil pore-fluid chemistry: Evidence from Santa Cruz, California. *Geochim.
841 Cosmochim. Acta* 74, 3883–3896. doi:10.1016/j.gca.2010.04.021
- 842 Tipper, E.T., Galy, A., Bickle, M.J., 2008. Calcium and magnesium isotope systematics in
843 rivers draining the Himalaya-Tibetan-Plateau region: Lithological or fractionation
844 control? *Geochim. Cosmochim. Acta* 72, 1057–1075. doi:10.1016/j.gca.2007.11.029
- 845 Tipper, E.T., Galy, A., Bickle, M.J., 2006. Riverine evidence for a fractionated reservoir of
846 Ca and Mg on the continents: Implications for the oceanic Ca cycle. *Earth Planet. Sci.
847 Lett.* 247, 267–279. doi:10.1016/j.epsl.2006.04.033
- 848 Uhlig, D., Schuessler, J.A., Bouchez, J., Dixon, J.L., Von Blanckenburg, F., 2017.
849 Quantifying nutrient uptake as driver of rock weathering in forest ecosystems by
850 magnesium stable isotopes. *Biogeosciences*. doi:10.5194/bg-14-3111-2017
- 851 Uroz, S., Calvaruso, C., Turpault, M.P., Frey-Klett, P., 2009. Mineral weathering by bacteria:
852 ecology, actors and mechanisms. *Trends Microbiol.* doi:10.1016/j.tim.2009.05.004
- 853 Vandevivere, P., Welch, S.A., Ullman, W.J., Kirchman, D.L., 1994. Enhanced dissolution of
854 silicate minerals by bacteria at near-neutral pH. *Microb. Ecol.* 27, 241–251.
855 doi:10.1007/BF00182408
- 856 Wakeman, C.A., Goodson, J.R., Zacharia, V.M., Winkler, W.C., 2014. Assessment of the
857 requirements for magnesium transporters in *Bacillus subtilis*. *J. Bacteriol.* 196, 1206–
858 1214. doi:10.1128/JB.01238-13
- 859 Welch, S. a., Ullman, W.J., 1999. The effect of microbial glucose metabolism on bytownite
860 feldspar dissolution rates between 5° and 35°C. *Geochim. Cosmochim. Acta* 63, 3247–
861 3259. doi:10.1016/S0016-7037(99)00248-3
- 862 Wiederhold, J.G., Kraemer, S.M., Teutsch, N., Borer, P.M., Halliday, A.N., Kretzschmar, R.,
863 2006. Iron isotope fractionation during proton-promoted, ligand-controlled, and
864 reductive dissolution of goethite. *Environ. Sci. Technol.* 40, 3787–3793.

865 doi:10.1021/es052228y

866 Wimpenny, J., Yin, Q.Z., Tollstrup, D., Xie, L.W., Sun, J., 2014. Using Mg isotope ratios to
867 trace Cenozoic weathering changes: A case study from the Chinese Loess Plateau.
868 Chem. Geol. 376, 31–43. doi:10.1016/j.chemgeo.2014.03.008

869 Wu, L., Jacobson, A.D., Hausner, M., 2008. Characterization of elemental release during
870 microbe-granite interactions at T = 28 °C. Geochim. Cosmochim. Acta 72, 1076–1095.
871 doi:10.1016/j.gca.2007.11.025

872 Zeev, A., Chien, M.W., 1991. Preconcentration technique for trace elements, CRC Press. ed.

873

FIGURE CAPTIONS

Figure 1.

Optical densities at 600 nm (a), glucose concentrations (b) and pH values (C) versus time for biotic experiments performed in reactors.

Figure 2.

Concentrations of organic acids versus time for R1 experiments performed with chelating RA1 and in B1 experiments performed with the acidifying PS2 strain.

Figure 3.

Fraction of Mg leached into solution from phlogopite versus time for bio- and chemical leaching experiments, as described in section 2.3.2.

Figure 4.

Ratios of elements released (Mg and Si), together with the elemental ratios of the initial phlogopite, as functions of time

Figure 5.

Mg release rates versus pH for all experimental reactors.

Figure 6.

$\delta^{26}\text{Mg}_{\text{DSM3}}$ values versus pH for all experimental reactors.

Figure 1

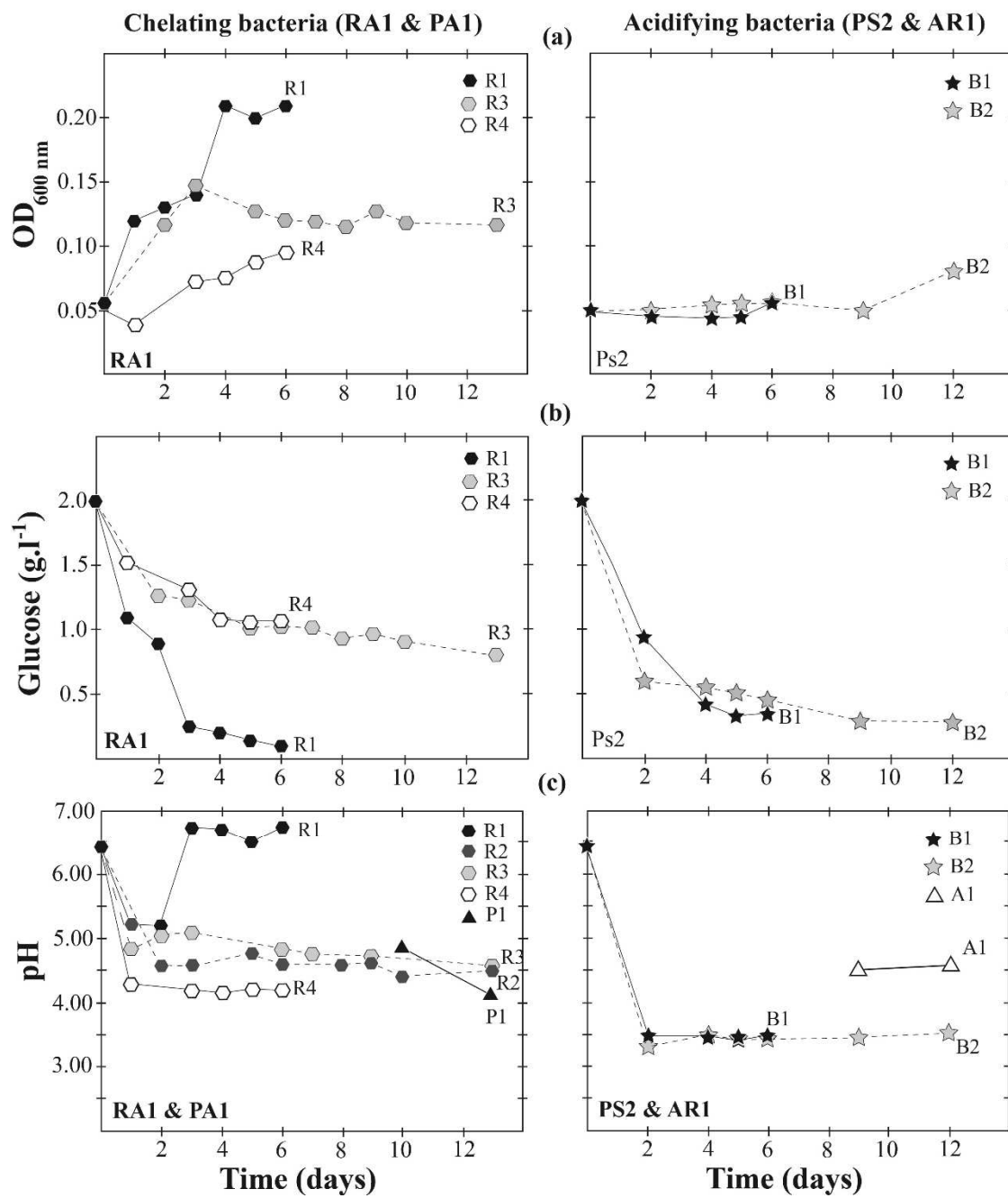


Figure 2.

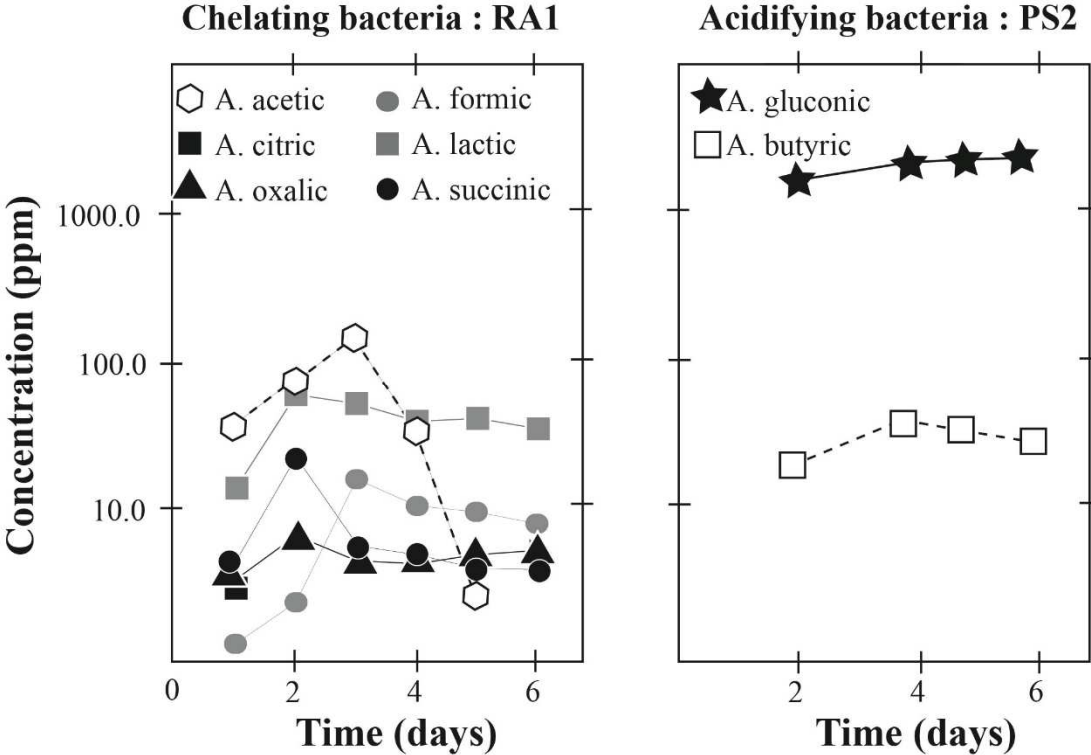


Figure 3.

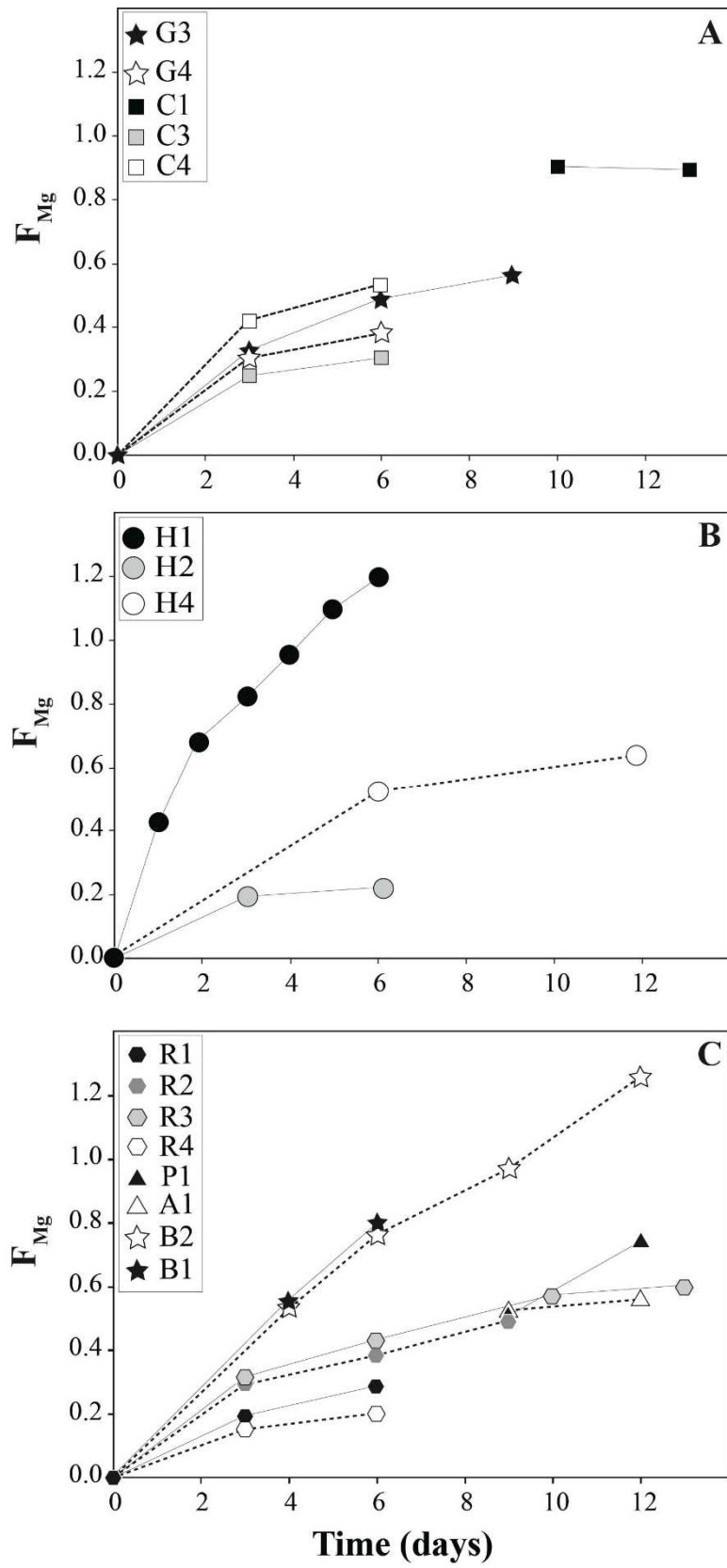


Figure 4.

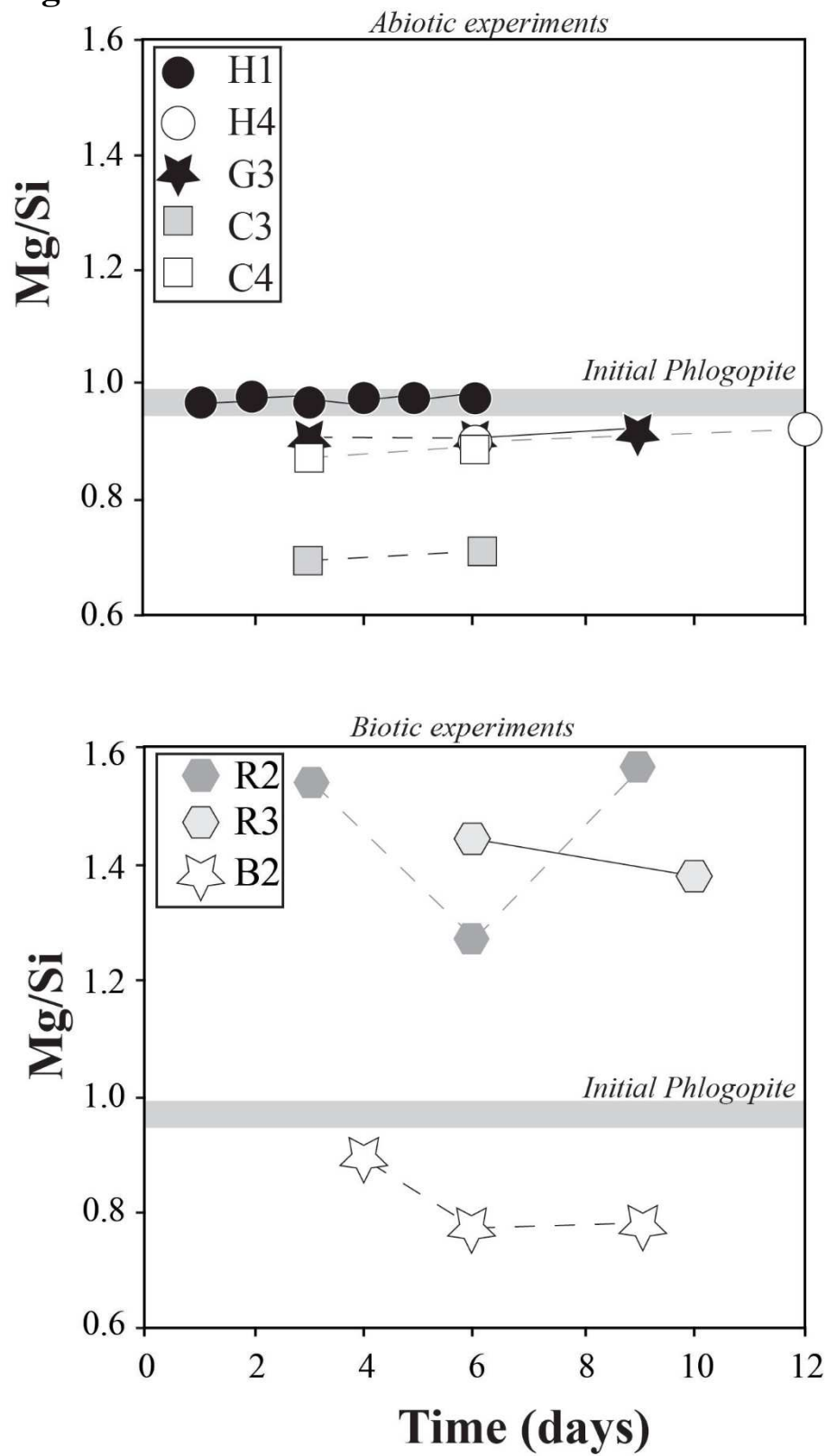


Figure 5.

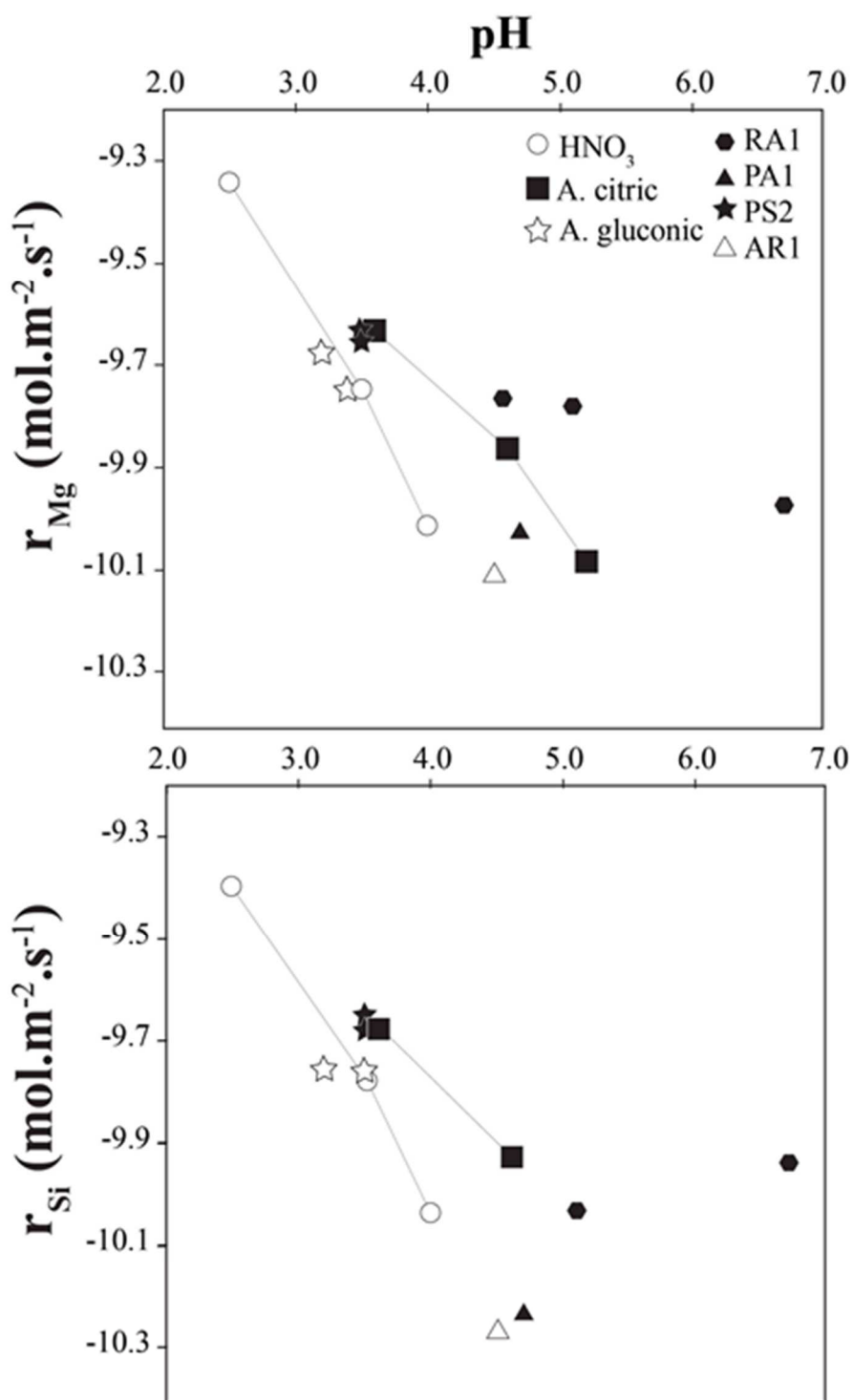


Figure 6.

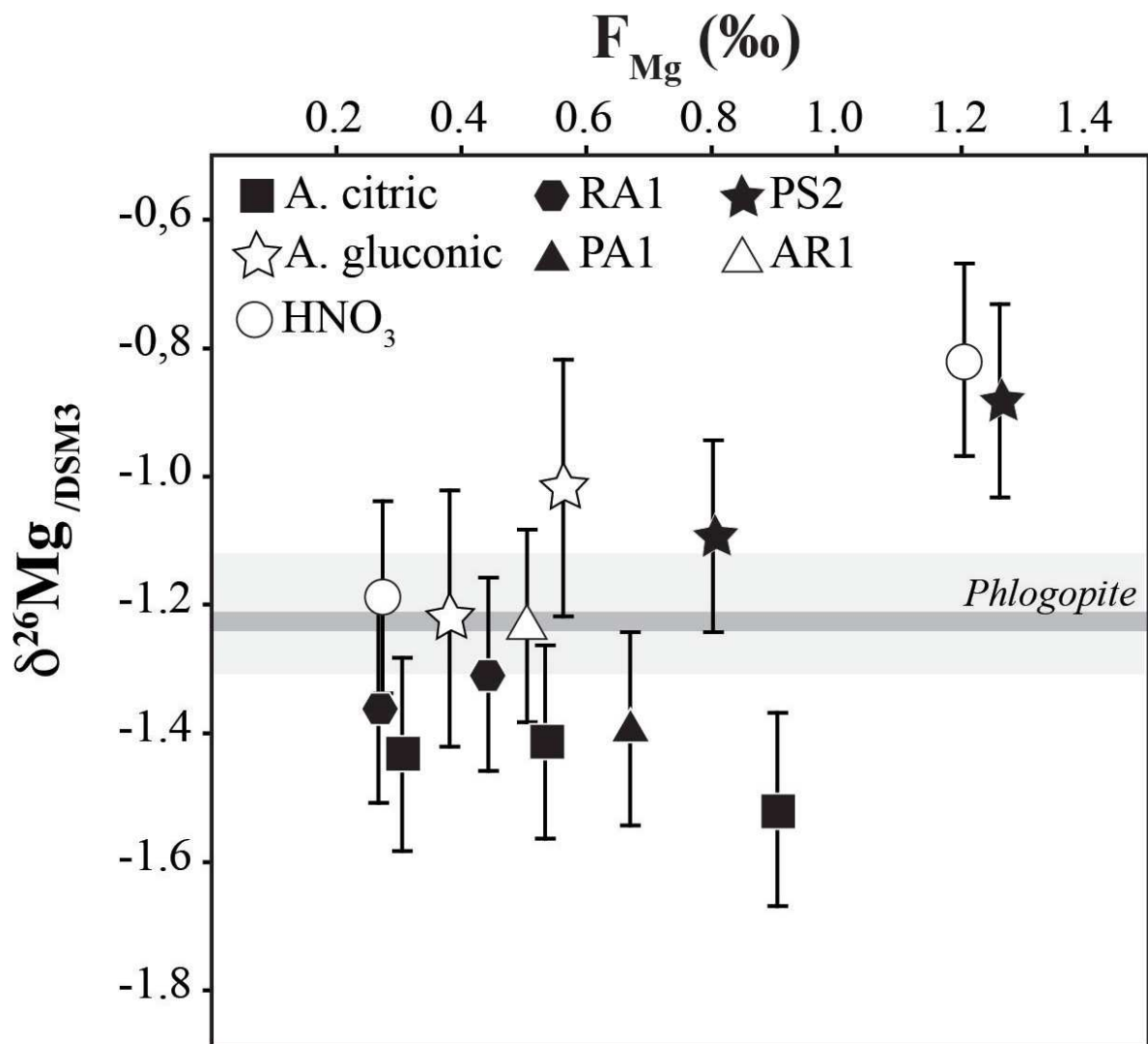
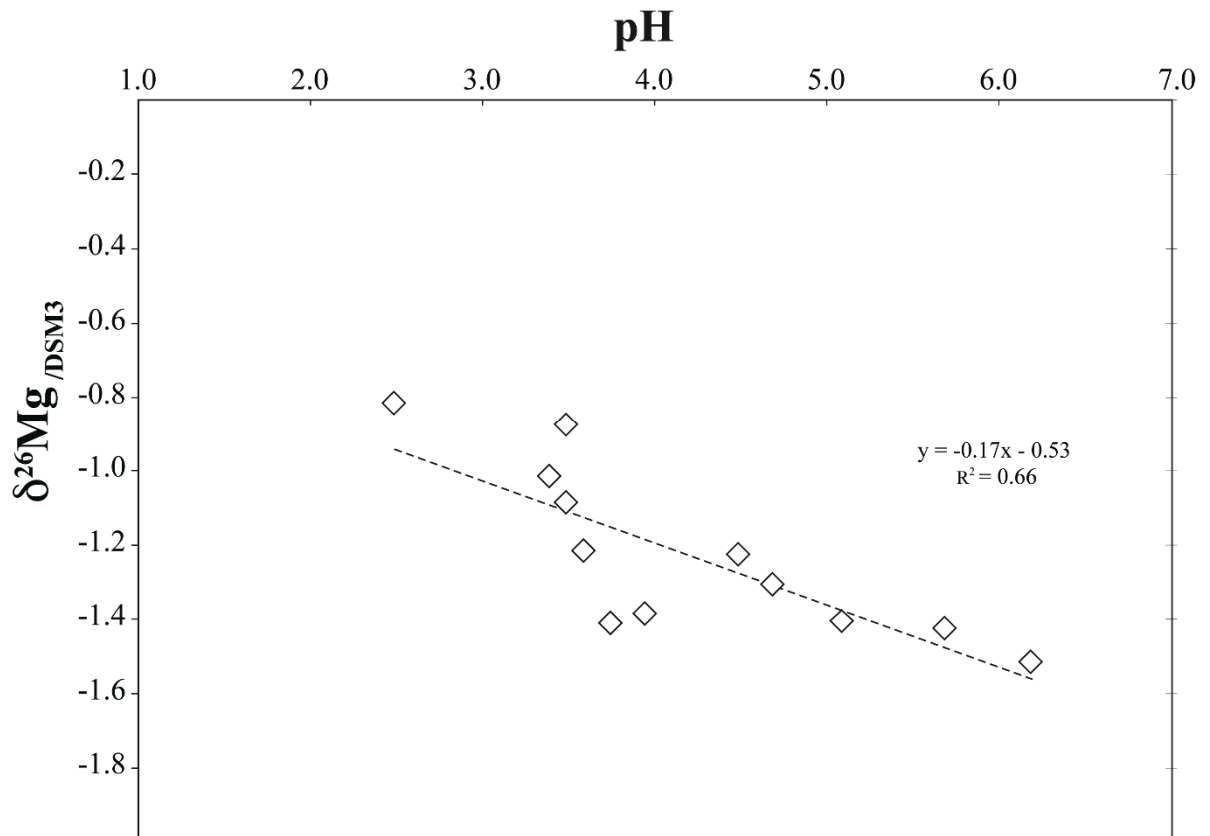


Figure 7.



1

TABLE CAPTIONS

Table 1.

General characteristics of reactor solutions in biotic conditions and abiotic conditions.

* “ppm”; “-” below detection

\$ MC-ICP-MS data were obtained using the Nu instrument (ENS, Lyon, with a 2σ external precision of 0.15%). Data in italics were obtained using the Isoprobe (CRPG, Nancy, with a 2σ external precision of 0.20%). Reported values represent the means of two or more replicate analyses of each sample. "#": Organic acid concentration of 0.001 M; "##": organic acid concentration of 0.01 M; "###": organic acid concentration of 0.1 M

Table 2.

Composition of bioreactor medium with two bacterial strains (*Rhanella aquatilis* RA1 and *Pseudomonas sp.* PS2), including optical density at 600 nm, glucose remaining in solution and organic acids produced (i.e., gluconic, lactic, acetic, butyric, formic, succinic, oxalic and citric acids).

TABLE 1.

Weathering agent	Experiments names	Times (day)	pH	Mg *	Si *	Mg/Si	$\delta^{26} \text{Mg}_{\text{DSM3}}^{\$}$	$\delta^{25} \text{Mg}_{\text{DSM3}}^{\$}$	$\Delta^{26} \text{Mg}_{(\text{solution-solid})}$
	phlogopite						-1.22 +/- 0.08	-0.62 +/- 0.08	
HNO ₃	H1	6	2.5	6.30	6.41	0.98	-0.82 +/- 0.02	-0.42 +/- 0.06	0.40
HNO ₃	H2	3	4.0	0.92	1.01	0.91			
		6	4.0	1.08	1.18	0.91			
HNO ₃	H3	9	5.6	1.44					
HNO ₃	H4	6	3.6	2.70	3.01	0.89			
		12	3.5	3.30	3.60	0.92			
gluconate ^{##}	G1	3	3.2	2.00	1.93	1.04			
		6	3.5	2.35	2.25	1.04			
gluconate ^{##}	G3	3	3.5	1.70	1.89	0.90			
		6	3.4	2.55	2.81	0.91			
		9	3.4	2.95	3.23	0.91	-1.02 +/- 0.25	-0.51 +/- 0.09	0.20
gluconate [#]	G4	3	3.6	1.60	1.75	0.91			
		6	3.6	2	2.18	0.92	-1.22 +/- 0.05	-0.63 +/- 0.06	0.00
citrate [#]	C1	10	5.7	4.74	5.06	0.94			
		13	6.2	4.70	5.29	0.89	-1.52 +/- 0.06	-0.78 +/- 0.09	-0.30
citrate [#]	C3	3	4.6	1.30	1.28	1.01			
		6	5.7	1.60	1.68	0.95	-1.43 +/- 0.02	-0.74 +/- 0.02	-0.21
citrate [#]	C4	3	3.6	2.20	2.31	0.95			
		6	3.6	2.80	3.01	0.93	-1.42 +/- 0.07	-0.73 +/- 0.07	-0.21
citrate ^{##}	C5	3	5.3	1.10	2.01	0.55			
		6	5.2	1.50	2.69	0.55			
citrate ^{###}	C6	3	5.3	1.20	2.11	0.57			
		6	5.3	1.60	2.78	0.57			
RA1	R1	3	6.7	1.00	1.25	0.8			
		6	6.7	1.50	1.61	0.93			

RA1	R2	3	5.1	1.56	1.01	1.54	-1.41 +/- 0.07	-0.73 +/- 0.09	-0.19
		6	4.8	2.01	1.58	1.27			
		9	4.7	2.58	1.65	1.56			
RA1	R3	6	4.6	2.26	1.57	1.44			
		10	4.4	2.98	2.15	1.38			
RA1	R4	6	4.2	1.05	1.20	0.875			
PA1	P1	9	4.7	2.67	1.90	1.4	-1.39 +/- 0.09	-0.72 +/- 0.09	-0.17
		12	3.9	3.90	3.06	1.27			
AR1	A1	9	4.5	2.76	2.12	1.30	-1.23 +/- 0.03	-0.63 +/- 0.06	-0.01
		12	4.5	2.94	2.35	1.26			
PS2	B1	4	3.5	2.90	3.23	0.90	-1.09 +/- 0.03	-0.56 +/- 0.07	0.11
		6	3.5	4.20	5.48	0.77			
PS2	B2	4	3.5	2.80	3.12	0.89	-0.88 +/- 0.05	-0.45 +/- 0.08	0.36
		6	3.5	4	5.16	0.77			
		9	3.5	5.1	6.56	0.77			
		12	3.5	6.60	8.49	0.78			

TABLE 2

Bacterial strains	Experiments names	Times (day)	OD _{600 nm}	glc *	Gluconate *	Lactate *	Acetate *	Butyrate *	Formate *	Succinate *	Oxalate *	Citrate *
RA1	R1	1	0.120	1100	-	15.0	38.3	-	1.3	4.7	3.4	3.1
		2	0.125	900	-	62.0	77.1	-	2.5	23.5	7.2	-
		3	0.140	250	-	54.2	152.4	-	16.8	6.2	4.9	-
		4	0.210	200	-	41.0	36.8	-	11.0	5.3	4.7	-
		5	0.200	150	-	43.1	2.9	-	9.8	4.3	5.1	-
		6	0.210	100	-	37.1	0.0	-	8.3	4.2	5.4	-
RA1	R3	2	0.118	1261								
		3	0.147	1231								
		5	0.127	1017								
		6	0.120	1020								
		9	0.127	970								
		10	0.118	900								
RA1	R4	5	0.091	1080								
		6	0.096	1070								
PS2	B1	2	0.050	940	1400.8	-	-	2.4	-	-	-	-
		4	0.043	640	1635.3	-	-	4.4	-	-	-	-
		6	0.055	420	1675.2	-	-	4.7	-	-	-	-
PS2	B2	2	0.050	600	1607.8	-	-	2.1	-	-	-	-
		4	0.054	450	2155.7	-	-	3.9	-	-	-	-
		6	0.055	290	2360.1	-	-	3.1	-	-	-	-
		9	0.050	280	2257.5	-	-	2.6	-	-	-	-
		12	0.080	260	2486.4	-	-	5.4	-	-	-	-